Sub-Optimal Control of Transient Non-Isothermal Viscoelastic Fluid Flows *

X. Marduel[†] , K. Kunisch[‡]

December 6, 1999

Abstract

Sub-optimal control of transient viscoelastic fluid flows in a 4 to 1 planar contracting channel is investigated. The control mechanism is based on heating or cooling the fluid along a portion of the boundary of the flow domain. In order to perform the control, a non-isothermal model for viscoelastic fluids is used consisting of the PTT model with relaxation time and elastic viscosity depending on temperature (following an exponential dependency, the WLF model). Moreover, the momentum, mass and constitutive equations are coupled with the heat equation forming the so-called primal system. The goal of the control is to reduce the large recirculation zones at the corners of the contraction. The sub-optimal strategy utilised for this purpose is the so-called "instantaneous control" method.

Keywords : Sub-Optimal Control, Instantaneous Control, Adjoint System, Finite Differences, PTT Model, Non-Isothermal Flows, Viscoelastic Flow, Transient Flow.

1 Introduction

Dealing with transient flow control, optimal control strategies are sometimes difficult on account of the size of the system of governing equations. The underlying algorithms to solve numerically these problems can be very complex and require a large amount of computational time and memory. Because of these difficulties, sub-optimal strategies are of interest. Though the control which will be found is not optimal, it can still be satisfactory in that the design objective is achieved. Several choices of sub-optimal strategies are possible. Among them, the instantaneous control method and its variants([4],[16], [5],[6],[11]), and reduced basis methods ([12],[13],[14],[17],[22],[25]).

In this work we shall utilise the instantaneous control strategy. As we are looking for controlling transient viscoelastic fluid flows, we consider a widely studied benchmark problem for such flows : the 4 to 1 contracting channel flow. The simple geometry of this flow domain is given in Figure 1.

*Supported in part by the SFB 03 "Optimierung und Kontrolle" through the "Fonds zur Förderung der wissenschaftlichen Forschung", Austria

†Institut für Mathematik, Karl-Franzens Universität Graz, Heinrichstraße 36, A-8020 Graz, Austria (xavier.marduel@kfunigraz.ac.at, http://www.kfunigraz.ac.at/imawww/marduel/).

‡Institut für Mathematik, Karl-Franzens Universität Graz, Heinrichstraße 36, A-8020 Graz, Austria (karl.kunisch@kfunigraz.ac.at).

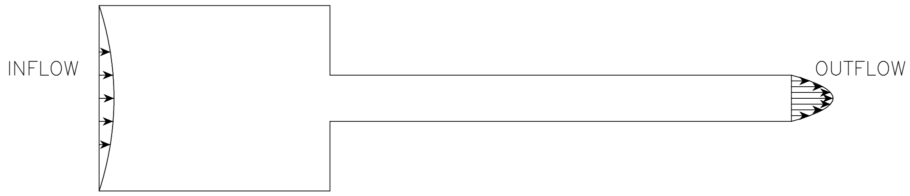

Fig 1: Domain of the flow

Numerical simulations in this domain have been challenging for a long time, especially for a high Weissenberg number, the non-dimensional number which quantifies the elasticity of the fluid. Indeed, the higher this number is, the more the singularity which occurs at the reentrant corners of the domain is exacerbated, leading to possible failures in numerical simulations. Another manifestation of the elastic character of the fluid are the large vortices which occur in the corners of the contraction. These are much bigger for Non-Newtonian than for Newtonian fluids and lead to a loss of energy of the fluid. Evaluating with precision the "Couette correction" which quantifies this loss of energy ([7]), as well as the intensity of the vortices, is also ones of the goals of numerical simulations. In recent years, great progress was made and new robust methods were developed. For finite element discretisations, we refer to [1][2] [3][8][10][23] for instance. Our method is based on finite difference discretisations. It is robust, efficient and precise. A natural objective in viscoelastic fluid flow control is to reduce the vortices in the fluid as much as possible, see Figure 4. For this purpose, we decide to act on the fluid by heating or cooling some part of the boundary of the flow domain. Indeed, non-isothermal effects are well known for their importance in viscoelastic fluid flows. Nevertheless, only a few non-isothermal simulations have yet been performed ([9], [19], [21], [24], [28], [30]). This is certainly due to the difficulties to model such flows : the heat transfer equation can be quite complex, as well as its coupling with the stress and momentum equations.
In [15] we utilised a simplified non-isothermal model for viscoelastic fluids. Considering stationary flows in this 4 to 1 contraction domain we were able to effectively reduce the recirculation zone and to minimise the related cost functionals chosen for this control problem. The objective of the present paper is to see if the approach used for stationary flows can be successfully applied for transient flows, and to analyse how the control and the resulting velocity field evolve in time. Finally, we also evaluate the performance of the instantaneous control method for the present problem.

The paper is organised as follows : we briefly recall in section 2 the set of equations which rules the flow of non-isothermal viscoelastic fluids. Then the optimality system for the optimal control problem is given in section 3, as well as its derivation in appendix **A**. In section 4 the instantaneous control strategy is introduced and the resulting optimality system is derived. Finally, numerical results are presented in section 5. We give our conclusions in section 6.

2 Problem statement

We denote by U the velocity of the fluid, p its pressure, $\boldsymbol{\tau}$ the stress tensor and T the temperature. The non-dimensional equations modeling the flow of viscoelastic fluids are given on one hand by the momentum (2.1) and mass (2.2) equations :

$$\mathrm{Re}[\ \frac{\partial U}{\partial t}\ +\ (U\cdot\nabla)\ U\ ] = -\nabla p + (1-\omega_r)\Delta U + \mathrm{Div}\ \boldsymbol{\tau} \quad , \tag{2.1}$$

$$\mathrm{div}\ U = 0 \qquad , \tag{2.2}$$

and on the other hand by a constitutive equation (2.3) which models the behavior of the fluid. The constitutive equation we choose is the linearised PTT [26] model :

$$\mathrm{We}(T)[\frac{\partial \boldsymbol{\tau}}{\partial t}\ +\ (U\cdot\nabla)\ \boldsymbol{\tau} - \nabla U\cdot\boldsymbol{\tau} - \boldsymbol{\tau}\cdot\nabla U^T\ ] + [1+\epsilon\frac{\mathrm{We}}{\omega_r}\mathrm{Tr}(\boldsymbol{\tau})]\boldsymbol{\tau} = 2\omega_r(T)\mathbf{D}\ . \tag{2.3}$$

In these equations, Re is the Reynolds number, We the Weissenberg number which quantifies the elasticity of the fluid, and $(1-\omega_r)$ (resp. ω_r) the Newtonian (resp. elastic) viscosity of the fluid. As we consider non-isothermal fluids, both the Weissenberg number and the elastic viscosity depend on temperature. The temperature dependency follows the WLF model [27],[29] :

$$\mathrm{We}(T) = \mathrm{We}\cdot f(T) \ \ , \ \ \omega_r(T) = \omega_r\cdot f(T) \quad \text{with} \quad f(T) = \frac{c_1\cdot T}{c_2+T}\ . \tag{2.4}$$

Finally, the heat equation (2.5) completes this set of equations :

$$\frac{\partial T}{\partial t}\ +\ (U\cdot\nabla)\ T = \frac{1}{\mathrm{Pe}}\Delta T \ \ , \tag{2.5}$$

where the Peclet number Pe is the ratio between heat convection and heat conduction. In this simplified heat transfer equation we neglect the terms due to viscous dissipation or viscoelastic phenomena. Indeed, these terms appear in the non-dimensional form of the equation in front of the coefficient $\frac{\mathrm{Br}}{\mathrm{Pe}}$, where Br is the Brinkmann number (see [15], [27] pg 85), which quantifies the ratio of viscous dissipation to heat conduction resulting from an imposed temperature difference. For flows related to the geometry of Figure 1, typical values of Br are small ([27], pg 78). Moreover, as we want to act on the flow by strongly heating or cooling the boundary of the domain to invoke a large temperature difference, the term $\frac{\mathrm{Br}}{\mathrm{Pe}}$ is negligeable. Finally, equations (2.1)-(2.5) have to be completed with boundary conditions to form the so-called primal system. These boundary conditions are depicted on Figure 2. Non-slip conditions ($U=0$) for the velocity are imposed on the wall of the flow

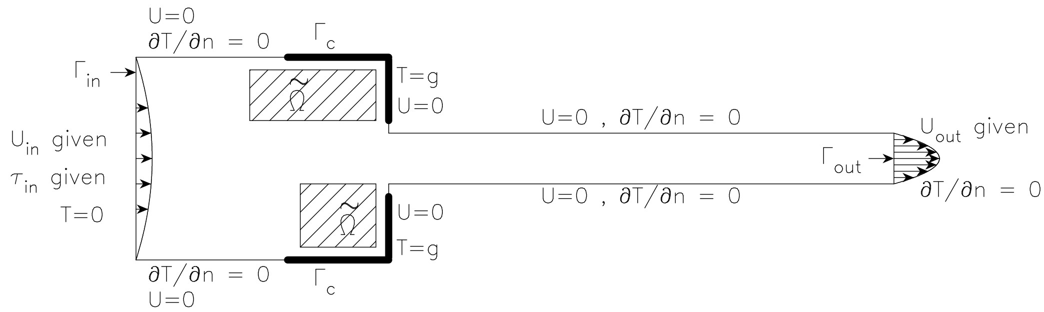

Fig 2: Domain with boundary conditions

domain, while at the entry Γ_{in} and the exit Γ_{out} of the domain fully developed Poiseuille flows are prescribed. The stress equation is of transport type : boundary conditions for $\boldsymbol{\tau}$ are only prescribed on the part of the boundary where $U \cdot n < 0$ (n being the normal exterior to the domain). In our configuration it reduces to Γ_{in}. Concerning the temperature T, we suppose that the fluid enters in the domain with a non dimensional temperature equal to zero. Thus we set $T = 0$ on Γ_{in}. The part of the boundary where we impose a control, called the "control boundary", is denoted by Γ_c. The control mechanism is described by the boundary condition

$$T = \mathbf{g} \qquad \text{on} \qquad \Gamma_c \ , \tag{2.6}$$

with $\mathbf{g}$ the control variable. Elsewhere on the boundary homogeneous Neumann conditions are given for T. Also depicted in Figure 2 is the so-called observation domain, denoted by $\tilde{\Omega}$. It is that part of the domain where measurements of the flow are assumed to be available. We next summerise the complete model which, in the context of control, is referred to as the primal system. The model is posed on the space-time cylinder $\Omega \times [0 : \mathfrak{T}]$, with Ω a bounded domain in $\mathbb{R}^2$ and $\mathfrak{T} > 0$ the final time.

$$(P) \begin{cases} \mathrm{Re}[\ \dfrac{\partial U}{\partial t} \ + \ (U \cdot \nabla)\ U\ ] = -\nabla p + (1-\omega_r)\Delta U + \mathrm{Div}\ \boldsymbol{\tau} \\[2ex] \mathrm{div}\ U = 0 \\[2ex] \mathrm{We}(T)[\dfrac{\partial \boldsymbol{\tau}}{\partial t} \ + \ (U \cdot \nabla)\ \boldsymbol{\tau} - \nabla U \cdot \boldsymbol{\tau} - \boldsymbol{\tau} \cdot \nabla U^T\ ] + [1 + \epsilon \dfrac{\mathrm{We}}{\omega_r} \mathrm{Tr}(\boldsymbol{\tau})]\boldsymbol{\tau} = 2\omega_r(T)\mathbf{D} \\[2ex] \dfrac{\partial T}{\partial t} \ + \ (U \cdot \nabla)\ T = \dfrac{1}{\mathrm{Pe}} \Delta T \\[2ex] \mathrm{We}(T) = \mathrm{We} \cdot f(T) \quad , \quad \omega_r(T) = \omega_r \cdot f(T) \quad . \\[2ex] \text{Boundary Conditions :} \\ \quad U = U_{in} \text{ on } \Gamma_{in} \times [0 : \mathfrak{T}] \qquad\qquad U = U_{out} \text{ on } \Gamma_{out} \times [0 : \mathfrak{T}] \\ \quad U = 0 \text{ elsewhere} \\[2ex] \quad \boldsymbol{\tau} = \boldsymbol{\tau}_{in} \text{ on } \Gamma_{in} \times [0 : \mathfrak{T}] \\[2ex] \quad T = 0 \text{ on } \Gamma_{in} \times [0 : \mathfrak{T}] \qquad\qquad T = \mathbf{g} \text{ on } \Gamma_c \times [0 : \mathfrak{T}] \\ \quad \dfrac{\partial T}{\partial n} = 0 \text{ on } \Gamma_n \times [0 : \mathfrak{T}] = \Gamma \setminus (\Gamma_{in} \cup \Gamma_c) \times [0 : \mathfrak{T}]. \\[2ex] \text{Initial Conditions :} \\ \quad U(t=0) = \ U_{ini} \quad \text{in } \Omega \\ \quad \boldsymbol{\tau}(t=0) = \ \boldsymbol{\tau}_{ini} \quad \text{on } \Omega \\ \quad T(t=0) = \ 0 \quad \text{in } \Omega\ . \end{cases}$$

The initial conditions U_{ini} and $\boldsymbol{\tau}_{ini}$ are taken as the numerical solution of the stationary equations with $\mathbf{g}=0$ (which implies $T=0$ in Ω), while the boundary conditions U_{in}, U_{out} and $\boldsymbol{\tau}_{in}$ are the velocity profile and the corresponding stress found by the numerical solution of a stationary Poiseuille flow.

3 The optimal control problem

The optimal control problem consists in minimising a functional $\mathcal{J}$ depending on the flow variables in $\tilde{\Omega}\times[0:\mathfrak{T}]$ and the boundary control $\mathbf{g}$. Here $\tilde{\Omega}$ denotes the observation domain. The choice of functionals must realise the control objective which consist in diminishing recirculation at the reentering corners of the domain. We shall mainly focus on the time-dependent version of two functionals that were already successful in the stationary case [15]:

$$\mathcal{J} \;=\; \mathcal{J}_1(U,\mathbf{g}) \;=\; \frac{\alpha}{2}\int_0^{\mathfrak{T}}\int_{\tilde{\Omega}} |U-U_{ns}|^2 \; dxdt \;+\; \frac{\ell}{2}\int_0^{\mathfrak{T}}\int_{\Gamma_c} |\mathbf{g}|^2 \; dxdt \quad , \tag{3.1}$$

$$\mathcal{J} \;=\; \mathcal{J}_2(U,\mathbf{g}) \;=\; \frac{\alpha}{2}\int_0^{\mathfrak{T}}\int_{\tilde{\Omega}} |\mathrm{Min}(0,u)|^2 \; dxdt \;+\; \frac{\ell}{2}\int_0^{\mathfrak{T}}\int_{\Gamma_c} |\mathbf{g}|^2 \; dxdt \quad , \tag{3.2}$$

where α and ℓ are two positive numbers which specify the cost of the state and control, U_{ns} stands for velocity field of the Newtonian fluid in the same domain, and $U=(u,v)$. The rational for the first choice of cost functional is the fact that Newtonian fluids develop no or only very small vortices in this 4:1 contraction flow domain. Trying to make the viscoelastic flow as near as possible to the Newtonian one is one way to reach our goal. The cost functional $\mathcal{J}_2$ on the other hand penalises negative contributions to the flow component in the longitudinal direction of the channel. If we succeed in reducing $\mathcal{J}_2$, then the flow should not develop regions where u is negative, which occurs in recirculation zones.

The optimal control problem can now be specified :

$$(Opt) \quad \begin{cases} \text{Minimize} \quad \mathcal{J}(U,\mathbf{g}) \\ \text{subject to} \quad U=U(\mathbf{g}) \quad \text{solution of } (P)\ . \end{cases}$$

A gradient algorithm to solve (Opt) is given by :

1. Set $k=0$ and choose $\mathbf{g}^0$ on $\Gamma_c\times[0:\mathfrak{T}]$ (e.g. $\mathbf{g}^0=0$)
2. Evaluate $\nabla\mathcal{J}(\mathbf{g}^k)$ on $\Gamma_c\times[0:\mathfrak{T}]$
3. Choose a descent step length $h>0$
4. Set $\mathbf{g}^{k+1}=\mathbf{g}^k - h\;\nabla\mathcal{J}(\mathbf{g}^k)$
5. Set $k\leftarrow k+1$, and goto 2

The formula for $\nabla\mathcal{J}(\mathbf{g}^k)$ is given by

$$\nabla\mathcal{J}(\mathbf{g}^k) = \frac{1}{\mathrm{Pe}}\partial_n\rho + \ell\,\mathbf{g}^k \qquad \text{on} \quad \Gamma_c\times[0:\mathfrak{T}] \tag{3.3}$$

where the "adjoint temperature" ρ is the solution of the adjoint system (D) with the variables $(\xi, \pi, \boldsymbol{\theta}, \rho)$. The adjoint system can be derived on the basis of (P) and $\mathcal{J}$ by means of Lagrange multipliers. The computations are given in Appendix **A**.

$$
(D)\left\{
\begin{array}{l}
\mathrm{Re}\,[\; -\dfrac{\partial \xi}{\partial t} - (U\cdot\nabla)\xi + \nabla U^T\cdot\xi\;] - (1-\omega_r)\Delta\xi - \nabla\pi = \\[2mm]
\qquad\qquad - \mathcal{J}_U - 2\dfrac{\omega_r}{\mathrm{We}}\mathrm{Div}\,\boldsymbol{\theta} - \left(\begin{array}{c}\partial_x\boldsymbol{\tau}:\boldsymbol{\theta}\\ \partial_y\boldsymbol{\tau}:\boldsymbol{\theta}\end{array}\right) - 2\,\mathrm{Div}\,(\boldsymbol{\theta}\boldsymbol{\tau}) - \rho\,\nabla T\;, \\[2mm]
\mathrm{div}\,\xi = 0\;, \\[2mm]
\mathrm{We}(T)[-\dfrac{\partial\boldsymbol{\theta}}{\partial t} - (U\cdot\nabla)\boldsymbol{\theta} - \boldsymbol{\theta}\cdot\nabla U - \nabla U^T\cdot\boldsymbol{\theta}\;] + \boldsymbol{\theta} + \epsilon\dfrac{\mathrm{We}}{\omega_r}[\mathrm{Tr}(\boldsymbol{\tau})\boldsymbol{\theta} + (\boldsymbol{\tau}:\boldsymbol{\theta})\mathbf{I}] = -\mathrm{We}(T)\,\mathbf{D}(\xi)\;, \\[2mm]
-\dfrac{\partial\rho}{\partial t} - (U\cdot\nabla)\rho - \dfrac{1}{\mathrm{Pe}}\Delta\rho + (\dfrac{1}{\mathrm{We}})'(T)[1+\epsilon\dfrac{\mathrm{We}}{\omega_r}\mathrm{Tr}(\boldsymbol{\tau})]\boldsymbol{\tau}:\boldsymbol{\theta} = 0\;. \\[2mm]
\text{Boundary Conditions :} \\
\quad \xi = 0 \text{ on } \Gamma\times[\mathfrak{T}:0] \\
\quad \boldsymbol{\theta} = 0 \text{ on } \Gamma_{out}\times[\mathfrak{T}:0] \\
\quad \rho = 0 \text{ on } (\Gamma_{in}\cup\Gamma_c)\times[\mathfrak{T}:0] \qquad \dfrac{1}{\mathrm{Pe}}\partial_n\rho = -u\rho \text{ on } \Gamma_{out}\times[\mathfrak{T}:0] \\
\qquad\qquad\qquad\qquad\qquad\qquad\quad \partial_n\rho = 0 \text{ on } (\Gamma\setminus\Gamma_{in}\cup\Gamma_c\cup\Gamma_{out})\times[\mathfrak{T}:0]\;. \\
\text{Final Conditions :} \\
\quad \xi\,(t=\mathfrak{T}) = 0 \text{ in } \Omega \\
\quad \boldsymbol{\theta}(t=\mathfrak{T}) = 0 \text{ on } \Gamma_{out} \\
\quad \rho(t=\mathfrak{T}) = 0 \text{ in } \Omega\;.
\end{array}
\right.
$$

Note that (P) and (D) are strongly coupled and in particular that while the equations in (P) are initial value problems those of (D) need to be solved backwards in time. Thus the evaluation of $\nabla\mathcal{J}(\mathbf{g}^k)$ requires the simultaneous solution of (P) and (D) on $\Omega\times[0:\mathfrak{T}]$. If we discretise (P) and (D) in time with an implicit Euler scheme for example, solving (P) requires the storage of $\mathbf{g}$ on $\Gamma_c\times[t_0;t_1;...;t_N]$, where t_n are the discretisation times and $N.\Delta t = \mathfrak{T}$, and the numerical resolution of (D) requires the storage of $(U,\boldsymbol{\tau},T)$ on $\Omega\times[t_0;t_1;...;t_N]$, which may be difficult. Moreover, since gradient algorithms are first-order methods, a high number of iterations can be required. Each gradient evaluation requires to solve (P) and (D). The resulting computational requirements may be beyond our workstations capacities. We therefore choose a sub-optimal control approach to solve our problem.

4 The sub-optimal control problem

As already mentioned, we choose the instantaneous control strategy to obtain a suboptimal solution for (Opt). It consists in discretising system (P) first with respect to a time discretisation $\{t_n\}_{n=1}^N$ (we choose the implicit Euler scheme), and then in solving at each time t_n a stationary optimal control problem:

(Opt^n) : Minimize $\mathcal{J}^n(U, \mathbf{g})$

where U is solution of the system (P^n):

$$(P^n) \quad \begin{cases} \mathrm{Re}[\ \dfrac{U - U^{n-1}}{\Delta t} + (U \cdot \nabla)\ U\ ] = -\nabla p + (1-\omega_r)\Delta U + \mathrm{Div}\ \boldsymbol{\tau} \quad , \\ \\ \mathrm{div}\ U = 0 \quad , \\ \\ \mathrm{We}(T)[\ \dfrac{\boldsymbol{\tau} - \boldsymbol{\tau}^{n-1}}{\Delta t} + (U \cdot \nabla)\ \boldsymbol{\tau} - \nabla U \cdot \boldsymbol{\tau} - \boldsymbol{\tau} \cdot \nabla U^T\ ] + [1 + \epsilon \dfrac{\mathrm{We}}{\omega_r} \mathrm{Tr}(\boldsymbol{\tau})]\boldsymbol{\tau} = 2\omega_r(T)\mathbf{D} \quad , \\ \\ \dfrac{T - T^{n-1}}{\Delta t} + (U \cdot \nabla)\ T = \dfrac{1}{\mathrm{Pe}} \Delta T \quad , \\ \\ \mathrm{We}(T) = \mathrm{We} \cdot f(T) \quad , \quad \omega_r(T) = \omega_r \cdot f(T) \quad . \\ \\ \text{Boundary Conditions :} \\ \quad U = U_{in} \text{ on } \Gamma_{in} \qquad\qquad U = U_{out} \text{ on } \Gamma_{out} \\ \quad U = 0 \text{ elsewhere} \\ \\ \quad \boldsymbol{\tau} = \boldsymbol{\tau}_{in} \text{ on } \Gamma_{in} \\ \\ \quad T = 0 \text{ on } \Gamma_{in} \qquad\qquad T = \mathbf{g} \text{ on } \Gamma_c \\ \quad \dfrac{\partial T}{\partial n} = 0 \text{ on } \ \Gamma_n \ = \Gamma \setminus (\Gamma_{in} \cup \Gamma_c) \ . \end{cases}$$

Here U^{n-1} is the solution of (P) at the $(n-1)^{th}$ time iteration (i.e. at time t_{n-1}), and U_{in}, U_{out} and $\boldsymbol{\tau}_{in}$ are given as in system (P).

The functionals $\mathcal{J}^n(U, \mathbf{g})$, corresponding to the 2 examples previously given have the form :

$$\mathcal{J}^n = \mathcal{J}_1^n(U, \mathbf{g}) \ = \ \frac{\alpha}{2} \int_{\tilde{\Omega}} |U - U_{ns}|^2 \ dx \ + \ \frac{\ell}{2} \int_{\Gamma_c} |\mathbf{g}|^2 \ dx \tag{4.1}$$

and

$$\mathcal{J}^n = \mathcal{J}_2^n(U, \mathbf{g}) \ = \ \frac{\alpha}{2} \int_{\tilde{\Omega}} |\mathrm{Min}(0, u)|^2 \ dx \ + \ \frac{\ell}{2} \int_{\Gamma_c} |\mathbf{g}|^2 \ dx \quad . \tag{4.2}$$

The practical minimisation of these functionals is again achieved with a gradient algorithm, with `maxit` denoting the maximum number of gradient iterations :

1. Set $k=0$ and choose $\mathbf{g}_0$ on Γ_c (e.g. $\mathbf{g}_0 = 0$)
2. Evaluate $\nabla \mathcal{J}^n(\mathbf{g}_k) = \frac{1}{\mathrm{Pe}}\partial_n\rho + \ell\, \mathbf{g}_k$ on Γ_c
3. Choose a descent step length $h > 0$
4. Set $\mathbf{g}^n_{k+1} = \mathbf{g}^n_k - h\, \nabla\mathcal{J}^n(\mathbf{g}^n_k)$
5. if $k < \mathtt{maxit}$, set $k \leftarrow k+1$, and goto 2

where the adjoint temperature ρ is the solution of the adjoint system (D^n) in the variables $(\xi, \pi, \boldsymbol{\theta}, \rho)$ related to (P^n) and $\mathcal{J}^n$:

$$
(D^n)\begin{cases}
\mathrm{Re}\ [\ \frac{\xi}{\Delta t} - (U\cdot\nabla)\xi + \nabla U^T\cdot\xi\ ] - (1-\omega_r)\Delta\xi - \nabla\pi = \\
\qquad -\ \mathcal{J}^n_U\ -\ 2\frac{\omega_r}{\mathrm{We}}\mathrm{Div}\ \boldsymbol{\theta}\ -\ \begin{pmatrix} \partial_x\boldsymbol{\tau} : \boldsymbol{\theta} \\ \partial_y\boldsymbol{\tau} : \boldsymbol{\theta} \end{pmatrix}\ -2\ \mathrm{Div}\ (\boldsymbol{\theta}\boldsymbol{\tau})\ -\ \rho\ \nabla T\ , \\
\mathrm{div}\ \xi = 0\ , \\
\mathrm{We}(T)[\ \frac{\boldsymbol{\theta}}{\Delta t} - (U\cdot\nabla)\boldsymbol{\theta} - \boldsymbol{\theta}\cdot\nabla U - \nabla U^T\cdot\boldsymbol{\theta}\ ]\ + \boldsymbol{\theta} + \epsilon\frac{\mathrm{We}}{\omega_r}[\mathrm{Tr}(\boldsymbol{\tau})\boldsymbol{\theta} + (\boldsymbol{\tau}:\boldsymbol{\theta})\mathbf{I}] = -\mathrm{We}(T)\ \mathbf{D}(\xi)\ , \\
\frac{\rho}{\Delta t}\ -\ (U\cdot\nabla)\rho\ -\ \frac{1}{\mathrm{Pe}}\Delta\rho\ +\ (\frac{1}{\mathrm{We}})'(T)[1+\epsilon\frac{\mathrm{We}}{\omega_r}\mathrm{Tr}(\boldsymbol{\tau})]\boldsymbol{\tau}:\boldsymbol{\theta} = 0\ . \\
\text{Boundary conditions :} \\
\quad \xi = 0 \text{ on } \Gamma \\
\quad \boldsymbol{\theta} = 0 \text{ on } \Gamma_{out} \\
\quad \rho = 0 \text{ on } \Gamma_{in}\cup\Gamma_c\ ,\ \frac{1}{\mathrm{Pe}}\partial_n\rho = -u\rho \text{ on } \Gamma_{out}\ ,\ \partial_n\rho = 0 \text{ on } \Gamma\setminus(\Gamma_{in}\cup\Gamma_c\cup\Gamma_{out})\ .
\end{cases}
$$

The optimality condition is given by :

$$
(\mathrm{OC}) \qquad \ell\,\mathbf{g} = -\frac{1}{\mathrm{Pe}}\partial_n\rho \quad \text{on } \Gamma_c \quad . \tag{4.3}
$$

In (D^n), $\mathcal{J}^n_U$ represents the derivative of $\mathcal{J}^n$ with respect to U, and is given by :

$$
\mathcal{J}^n_U = \mathcal{J}^n_{1,U} = \quad \alpha\,(U - U_{ns})
$$

and

$$
\mathcal{J}^n_U = \mathcal{J}^n_{2,U} = \quad \alpha\,\mathrm{Min}(0,u)\quad .
$$

Returning for a moment to (Opt) we note that its solutions are independent of (α,ℓ)-pairs for which $\frac{\alpha}{\ell} = constant$. The merit in allowing independent weights for the formulation of $\mathcal{J}$ lies in the effect of scaling the adjoint variables by α as can be seen from the formulas for $\mathcal{J}^n_U$ and (D^n). Since in our numerical examples $\mathcal{J}^n_U$ is frequently very small, choosing $\alpha > 1$ facilitates the computations of the adjoint equations and of the term $\frac{1}{\mathrm{Pe}}\partial_n\rho$. (Without the scaling and with $\partial_n\rho$ computed from $\mathcal{J}^n_U$ with $\alpha = 1$, we would have to postmultiply $\partial_n\rho$

by α to obtain the same expression for the gradient as describe above).

Now we give the flow-chart of the complete algorithm for the sub-optimal control strategy on $[0:\mathfrak{T}]$:

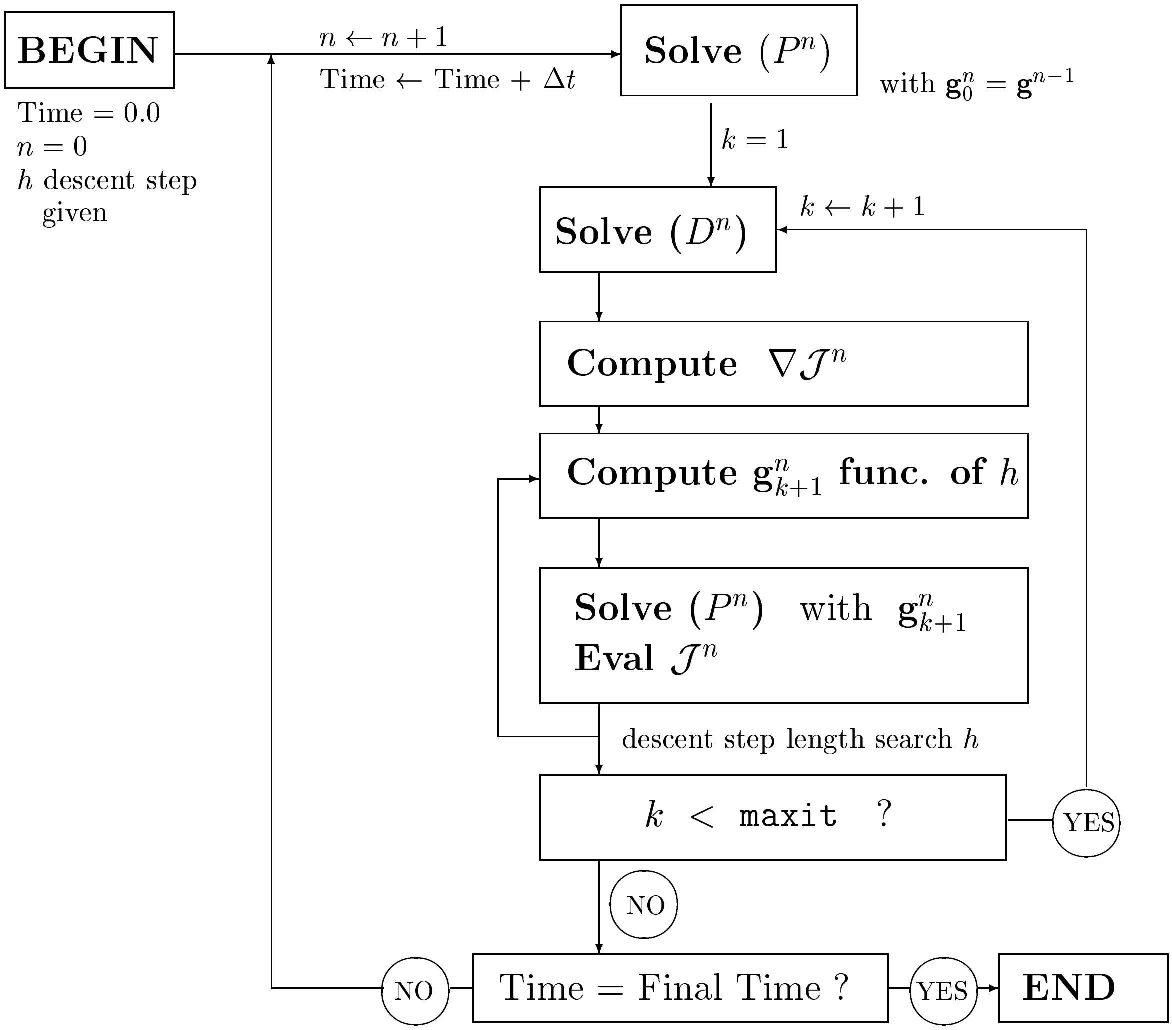

The inner loop "descent step length search" consists in finding a good choice for the descent step h in step 4 of the gradient algorithm in order to update efficiently the control :

$$\mathbf{g}_{k+1}^n = \mathbf{g}_{k+1}^n(h) = \mathbf{g}_k^n - h\ \nabla \mathcal{J}^n(\mathbf{g}_k^n). \tag{4.4}$$

For this purpose, we proceed with an interpolation procedure. Given an initial guess h (the one of the previous time iteration), we evaluate $\mathbf{g}_{k+1}^n(0), \mathbf{g}_{k+1}^n(h), \mathbf{g}_{k+1}^n(h/2)$ with (4.4), and solve with these 3 controls the system (P), which provides 3 costs $\mathcal{J}^n(0), \mathcal{J}^n(h), \mathcal{J}^n(h/2)$. The cost $\mathcal{J}^n$ as a function of h is interpolated between these 3 values, and the step length h is chosen as the value of the minimizer of the quadratic interpolation. This procedure requires to solve (P) 4 times in each gradient iteration. Although it is costly it always provided a good decrease of the cost functional $\mathcal{J}^n$, if $\mathbf{g}_{k+1}^n$ gives a descent direction. In the case where $\mathcal{J}^n(h) > \mathcal{J}^n(0)$, we don't make any step descent length search and let the cost increase at this time iteration.

5 Numerical results

5.1 Solution Method

We briefly describe the numerical methods that we employ. The method of resolution of (P) and (D) is based on a finite difference discretisation on staggered grids, and a Gauss-Seidel solver together with a multigrid algorithm. Here we give in Figure 5.1 the staggered grids for the "primal unknowns". For the variables of the adjoint system the same locations are used.

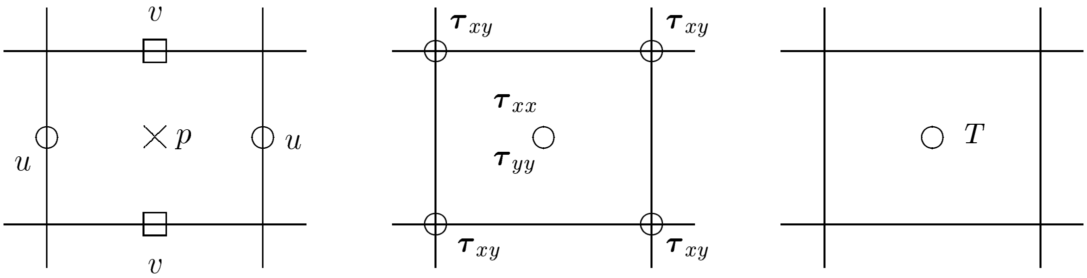

The location of the unknowns on these staggered grids allows us to compute in a precise way all the convection terms which arise in all the equations, which is a key point in numerical calculations for viscoelastic fluid flows. The flowchart of the Gauss-Seidel algorithm-like we utilise is given in Figure 3 : We denote by Res_U ($Res_{\boldsymbol{\tau}}$,Res_T) the residual of the equation

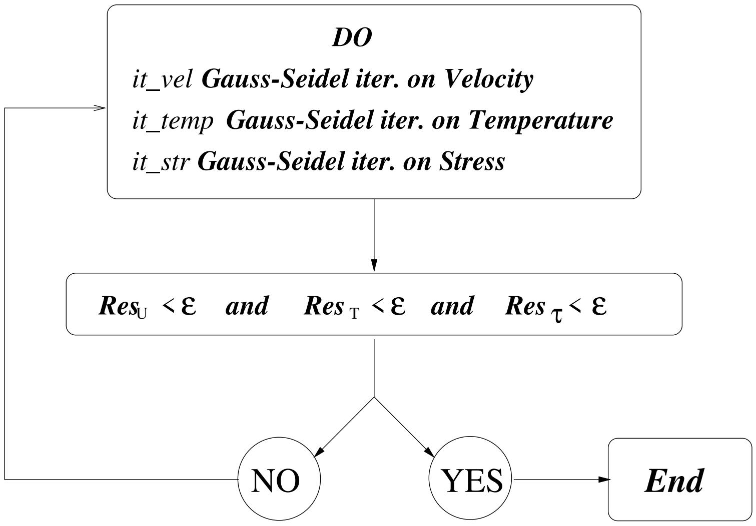

Fig 3: Gauss-Seidel Algorithm on one grid

on velocity (stress, temperature). As indicated on Figure 3, we perform *it_vel* Gauss-Seidel iterations on the momentum equation, considering fixed $\boldsymbol{\tau}$ and T, then *it_temp* iterations on the heat equation, with fixed U and $\boldsymbol{\tau}$, and finally *it_str* iterations on the stress equation, this time with fixed U and T. Our algorithm follows a "decoupled approach", but small values for *it_vel*, *it_temp* and *it_str* introduce a strong coupling between the three equations in the numerical computation. As a result, computational time for the resolution of the system is lowered, and the method is also much more robust. These features are kept with the "FAS" multigrid algorithm we employ. To solve the adjoint system, we keep the same grid as for the primal system. Nevertheless, a slightly modified method is necessary to solve the adjoint equation : we have to take into account the direction of the flow. For the primal variables, the quantities $\boldsymbol{\tau}$ and T are convected with the velocity $U > 0$, i.e. from the left to the right. Thus for an efficient Gauss-Seidel solver, unknowns are enumerated from the left to the right. Concerning the adjoint variables, quantities are convected with $-U$, and we enumerated the unknowns from the right to the left. The dual heat equation is also of a different kind as its primal counterpart, because of the so-called Robin boundary conditions on Γ_{out}. This means that at Γ_{out} (the "entry" for the dual variables), ρ is unknown . To solve this equation, we perform Gauss-Seidel iterations from the right to the left (with an a-priori ρ), and then from the left to the right. More details of the method can be found in [15] and [20].

Let us describe the numerical validation that was carried out. At each time step, we control the precision of our computations with the stopping criteria $Res_U < \epsilon$, $Res_{\boldsymbol{\tau}} < \epsilon$, $Res_T < \epsilon$. It turns out that $\epsilon = 10^{-5}$ is sufficient, and that at each time iteration we are able to satisfy it. The validation of the scheme can only be given through numerical tests (mesh independence, time step refinements) as for our geometry no analytical solutions exist with respect to which we could compare our results. For stationary flows, we utilized in [15] the present computational grid (which for viscoelastic fluid flows computations is a rather fine grid) and a second one, twice finer. The results were the same. Once we gained confidence in the spatial resolution, we solved the primal system with different time steps and checked the solutions we obtained starting from a state at rest. We reached the same stationary state at the same speed for all time steps $\Delta t < 0.1$ (remember that the flow is "slow", the Reynolds we employ being very small due to the relation $\mathrm{Pe} = \mathrm{Re}\ \mathrm{Pr}$ where Pr is the Prandlt number). The value of $\mathrm{Pr} = \frac{\nu}{\hat{\alpha}}$ depends only on the physical quantities ν the fluid's viscosity and $\hat{\alpha}$, the thermal diffusivity. Typical values of Pr are $\mathrm{Pr} = 10^7$, so if we choose $\mathrm{Pe} = 100$ then $\mathrm{Re} = 10^{-5}$. In Figure 10 the results of simulations for two different Δt, one with $\Delta t = 0.1$, an other with $\Delta t = 0.05$, while all other parameters remain unchanged, are given. While the final controlled flows are quite similar, the controls themselves and the cost functional differ as a result of the frequency by which the controls are computed.

5.2 Tests

The instantaneous control technique is a heuristic that has proved to be successful in various large scale evolutionary optimal control problems. Its behavior for (Opt) is not a priori clear and with present analytical results it cannot be predicted for which cost functional the control objective of reducing the vortices would be achieved. In our experiments the control objective was not reached when utilising $\mathcal{J}_1$. We recall here that $\mathcal{J}_1$ was quite successful for control of stationary problems [15]. For $\mathcal{J}_2$ the results for evolutionary problems were quite successful and therefore we give results only for this case.

We choose as values for the PTT model parameters $\epsilon = 0.02$, $\mathrm{We} = 10$ or $\mathrm{We} = 20$, and $\omega_r = 0.89$, which are standard parameters in viscoelastic simulations. Unless specified otherwise, the discretisation time step is taken as $\Delta t = 0.1$. The initial condition $(U_0, p_0, \boldsymbol{\tau}_0, T_0)$ is the solution of the isothermal stationary problem. We give the resulting flows in Figure 4, for both We = 10 and We = 20. The domain of observation in chosen to be $\tilde{\Omega} = [-04.0 : -0.01] \times [-3.99 : +3.99]$, and the control boundary Γ_c is given by $\Gamma_c = [-10.0 : 0.00]$ on the horizontal walls of the upstream channel. On the vertical walls of the upstream channel, $\Gamma_c = [-4.0 : -1.2] \cup [1.2 : 4.0]$. (We set the abscissa 0.0 at the junction between the upstream-downstream channel, and the ordinate 0.0 on the horizontal axis of symmetry of the domain : Γ_c is taken symmetric with respect to the domain). Concerning the coefficients c_1 and c_2 of the WLF's function f, we take $c_1 = 15$ and $c_2 = 50$, which corresponds to a choice where We and ω_r vary strongly with T.

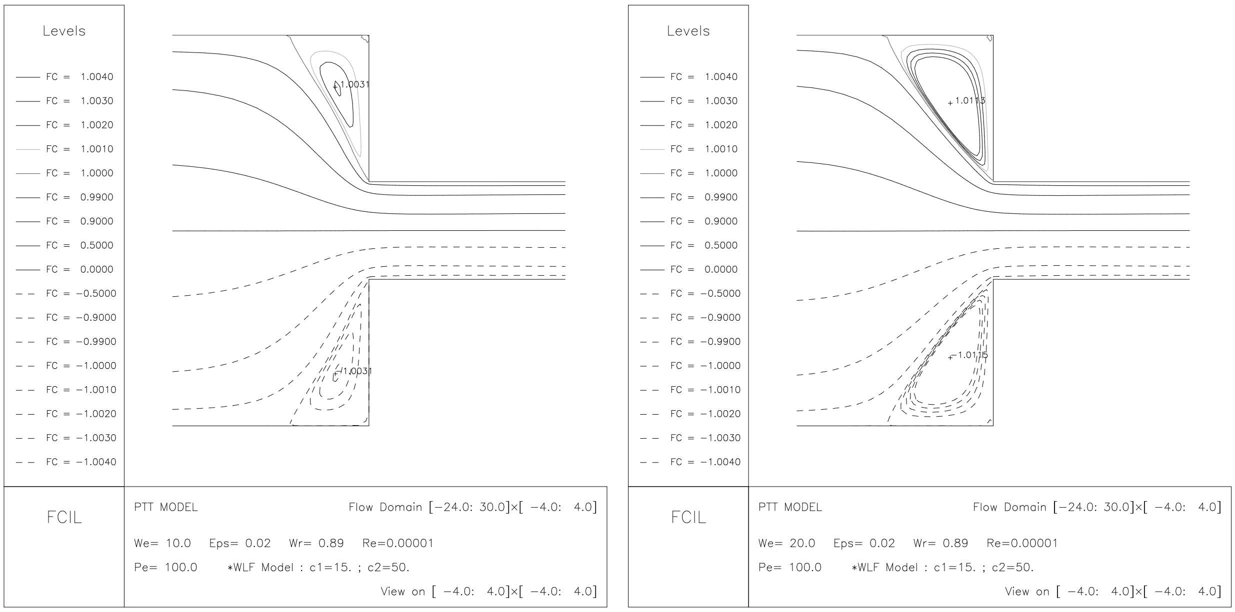

Fig 4: Streamlines of uncontrolled Flow ($T = 0$ in Ω) for We = 10 (left) and We = 20 (right).

For the first experiment that we report upon here we chose, in addition to the parameters already specified above, $\alpha = 10^8$, $\ell = 4 \times 10^{-4}$ and We = 10. No control is imposed until $t = 1.0$, which means during 10 time steps. This ensures that we start from a stationary flow : indeed, during these 10 time steps the flow is steady. Then from $t = 1.0$ until $t = 3.0$ the number of gradient iterations denoted `maxit` was set to 3 and line searches were carried out. Beyond $t = 3.0$ `maxit` was set to 1 and the step length was set constant based on previous experience. Let us briefly reflect on the size of the problem. Though the zone of interest is at the junction of the upstream-downstream channel, we have to utilise long channels for reasons of numerical stability. As indicated on Figure 4, the length of the upstream channel (resp. downstream channel) is set to 24.0 (resp. 30.0). The mesh must be particularly refined at the reentrant corners of the domain. Even with non-uniform grids the total number of cells is 7,860 for the mesh we utilise, which means about 50,000 unknowns for the primal system. The main difficulty for solving (P) is not the non-linearity which occurs in the stress equation, but the coupling between this equation and the momentum equation. The coupling between the heat and the stress equations does not add difficulties.

When `maxit` is set equal to 1 then at each time it is required to solve (P) twice and (D) once. The computing time to solve these 3 systems is on the order of one minute.

In Figures 5-7 we give the result for this test. On the top left of the Figures the stream-function (annotated "FCIL") is given, on the bottom left we find the cost functional, while top right and bottom right show the temperature field in the domain (annotated "HTIL") and the control at the time specified in the legend below the graph of the cost functional. Concerning the cost functional plot, the shaded bar at the top indicates the status of the cost function : no control (in grey), optimal control (black), negative of optimal control (light grey).

Note in Figure 8 that the value of the cost at $t = 1.0$, i.e. just before control is enforced for the first time, is $\mathcal{J} = 80.9$. The results we obtain after a small number of time iterations indicate a fast decrease of the cost functional. We note that while the vortex size has been reduced, the vortex itself is still present. The stream function denoted ϕ has been calculated such a way that $\phi = -1$ on the lower boundary and $\phi = +1$ on the upper boundary. Its value in the vortices has been reduced in absolute values from 1.0031 (Figure 4) to 1.0003, which infact leads to a strong reduction of the vortex size (Figure 5). The reattachment length X $= L_v/D_u$ is equal to 0.097, while X was equal to 0.138 for the uncontrolled flow (D_u is the upstream channel diameter and L_v the length of the vortex on the horizontal boundary of the upstream channel). At time $t = 600$ we decide to discontinue the control action and set $\mathbf{g} = 0$. As a consequence, recirculation reappears. Then at time $t = 700$ we enforce as control the negative of the temperature profile which was the optimal temperature control at $t = 600$. The intensity of the flow in the recirculation zone immediately increases. The mpeg animation of this simulation can be found at the web-address given on the first page.

Summarizing our experience with the instantaneous control strategy as depicted in Figures 5-7 it provides an effective method for thermal control for the viscoelastic fluid. The chances for success were not at all clear at the outset of our experiments.

- Gradient algorithm parameters :

We report on selected experiments concerning the influence of the number of gradient iterations on the qualitative behavior of the instantaneous control strategy. First we compare results of three tests. In test 1 we perform only one iteration at each time level and fix the descent parameter h on a previously determined successful value. In test 2 (which correspond to Figures 5-7) we perform line search with three gradient steps from $t = 1.0$ to $t = 3.0$, and switch to one gradient step without line search at $t = 3.0$. Finally in test 3 line searches with three gradient steps are performed from $t = 1.0$ to $t = 200.0$. In Figure 8 the values of the cost functionals for these three tests with the other parameters as above, are given. The graphs indicate no significant differences among the results for these three tests.
In a different set of tests we observed that big differences can occur when we start test 1 with bad choices of h, h too small for example. Then the line search permits to correct this bad initialisation of the descent length step, and to find the good order of magnitude required for it.

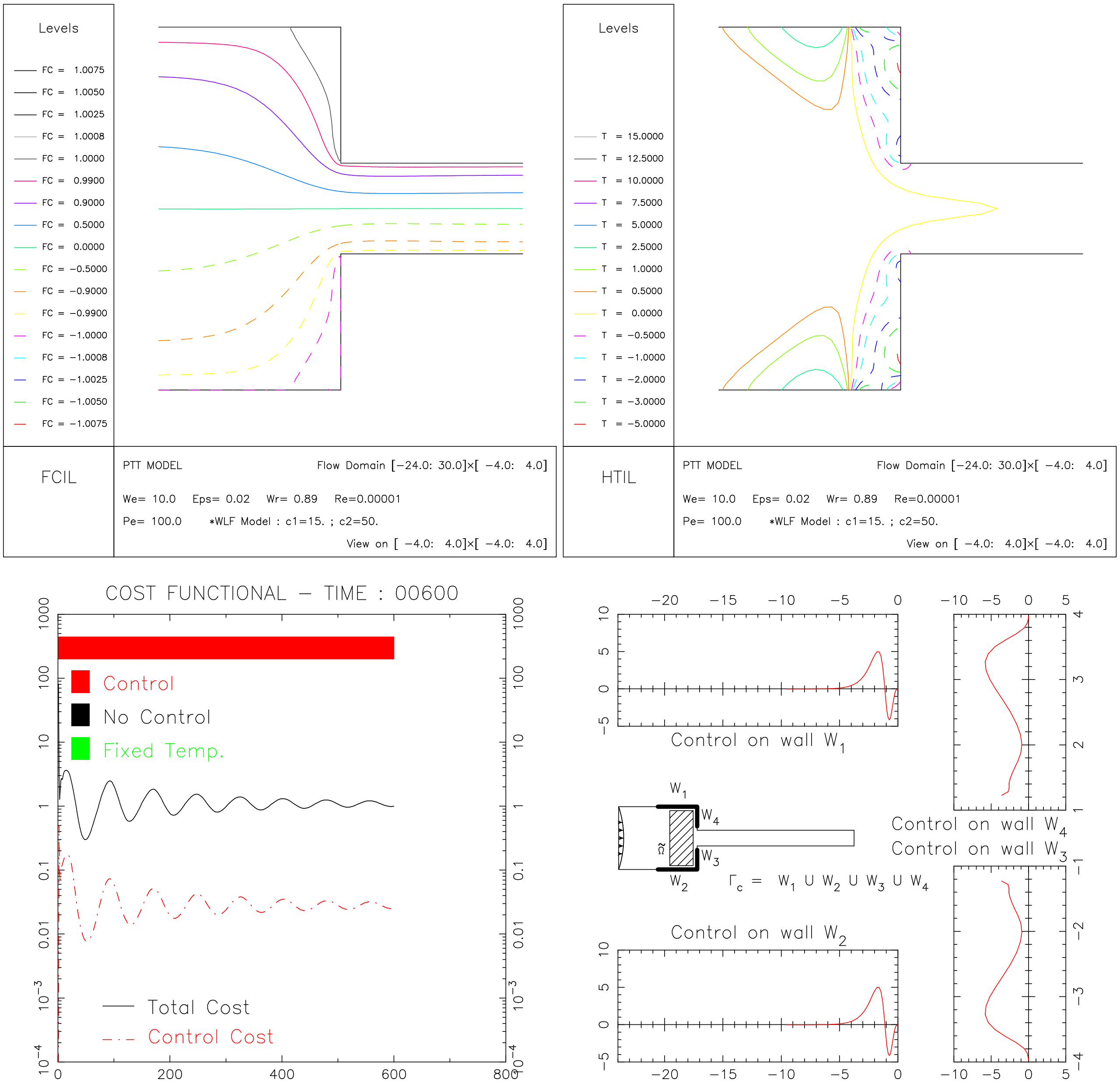

Fig 5: Simulation We $= 10$, $\ell = 4 \times 10^{-4}$ - Snapshot at $t = 600.0$

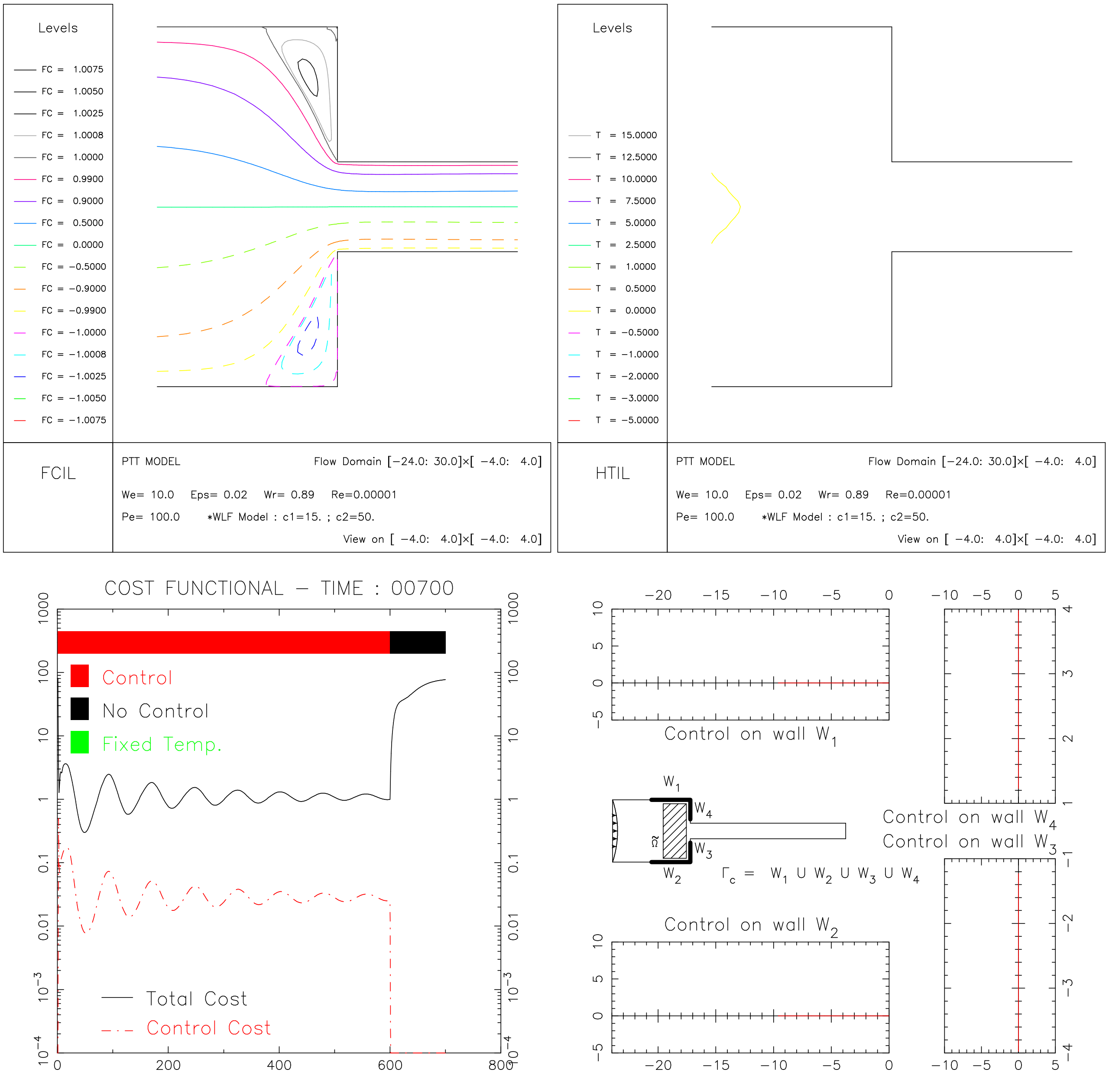

Fig 6: Simulation We $= 10$, $\ell = 4 \times 10^{-4}$ - Snapshot at $t = 700.0$

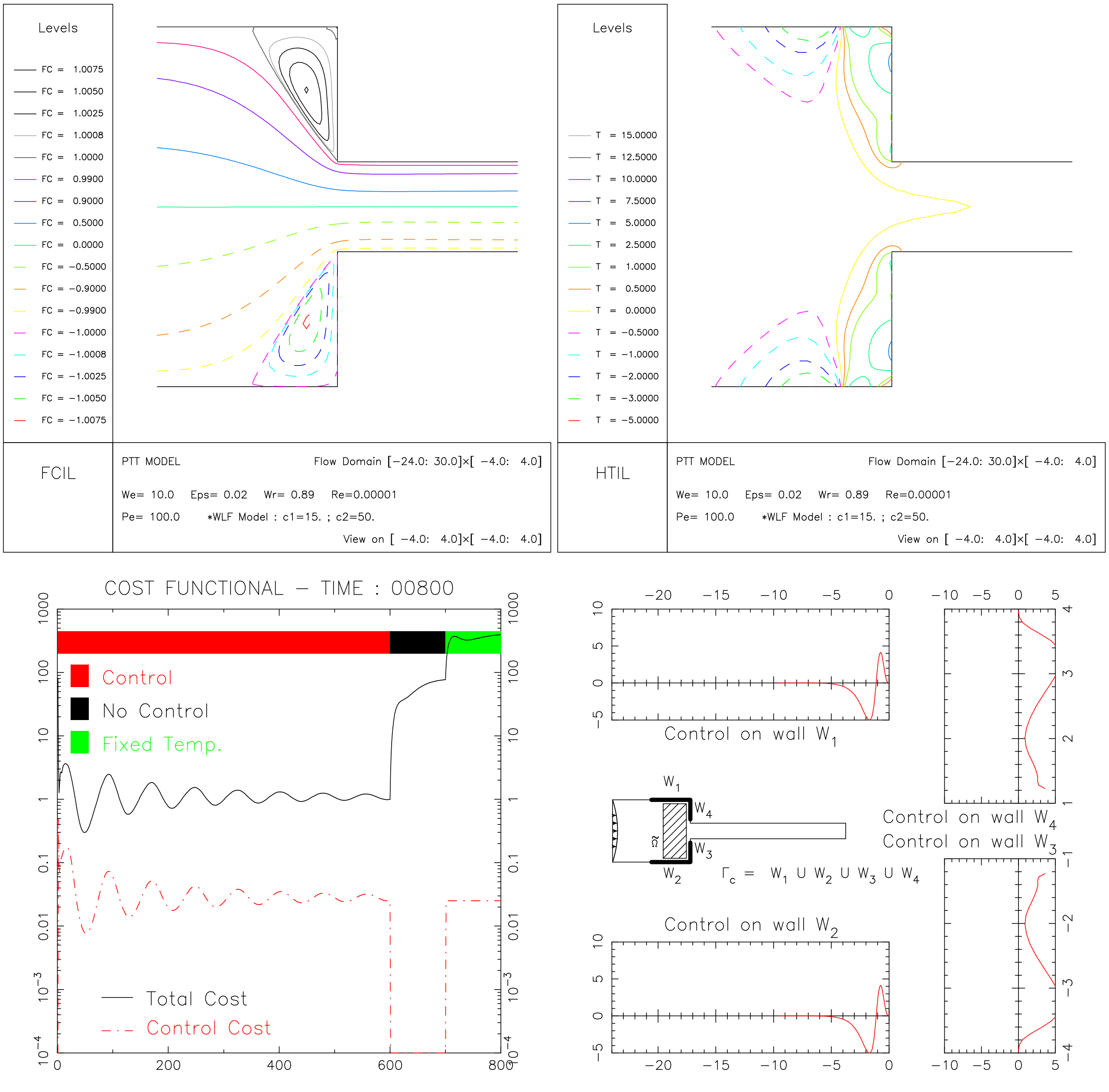

Fig 7: Simulation We $= 10$, $\ell = 4 \times 10^{-4}$ - Snapshot at $t = 800.0$

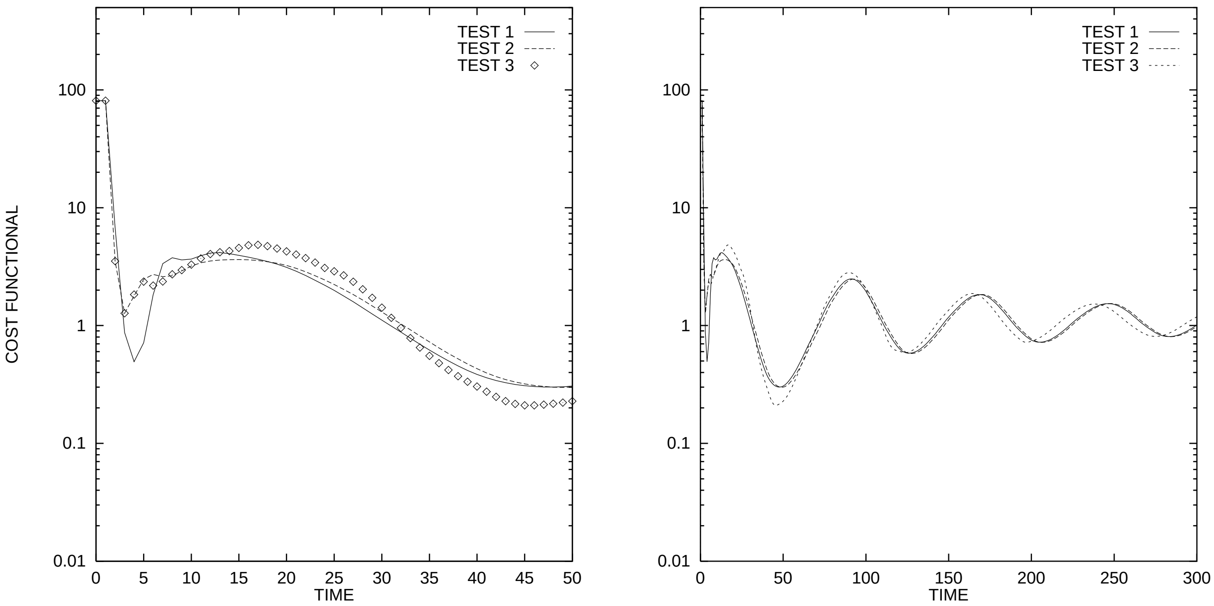

Fig 8: Cost until time $t = 50.0$ (left), $t = 300.0$ (right)

We can conclude here that for transient flows in the given test configuration, a well chosen descent step with only one gradient iteration gives as satisfactory results as line search procedures with many gradient iterations.

• Importance of the cost functional parameters α and ℓ :

It is essential to find a good balance between α and ℓ, the two weights in the cost functional. Note that this was also true for stationary simulations [15]. We carried out several tests to determine the best parameters, and the above choice of $\alpha = 10^8$ and $\ell = 4 \times 10^{-4}$ is in a certain sense a turning point as we shall demonstrate below. But first let us note that for fixed α the influence of ℓ is as expected: if ℓ is too large, then the control is too expensive to significantly influence the flow pattern. If ℓ is too small, then the control is too cheap with respect to the flow and it will vary a lot even if only small changes occur in the flow. In Figure 9 left, we give the evolution of the cost with 3 different values of ℓ : first with $\ell = 4 \times 10^{-4}$, then with $\ell = 2 \times 10^{-4}$, finally with $\ell = 10^{-4}$. The smaller ℓ is (for fixed α), the more the cost oscillates. For $\ell = 10^{-4}$ it was necessary to decrease the time step to $\Delta t = 0.05$ to obtain a stable control regime. In Figure 9 right, we show the results of simulations with a Weissenberg number of We = 20, which is a challengingly large value even for direct simulations. Here the parameters are $\alpha = 10^8$, $\ell = 10^{-4}$ for the test 1, $\alpha = 10^8$, $\ell = 2 \times 10^{-4}$ for the test 2, and $\alpha = 10^8$, $\ell = 10 \times 10^{-4}$ for test 3. Again the oscillations are reduced by increasing ℓ. Note that for We = 20, the initial cost is $\mathcal{J}_{\mathrm{We}\ 20} = 1167.4$, and the average cost of the controlled system is 1.0 .

Viewing the mpeg animations of these simulations, ones notes that we have constrained the control between the values $\mathbf{g}_{min} = -10.0$ and $\mathbf{g}_{max} = 30.0$. Indeed, the control can reach very high values at the beginning of the control process since it tends to act on the flow as soon as possible. This can lead to numerical crashes. Later on, when the control process is well established, the control assumes moderate values, and the constraints are

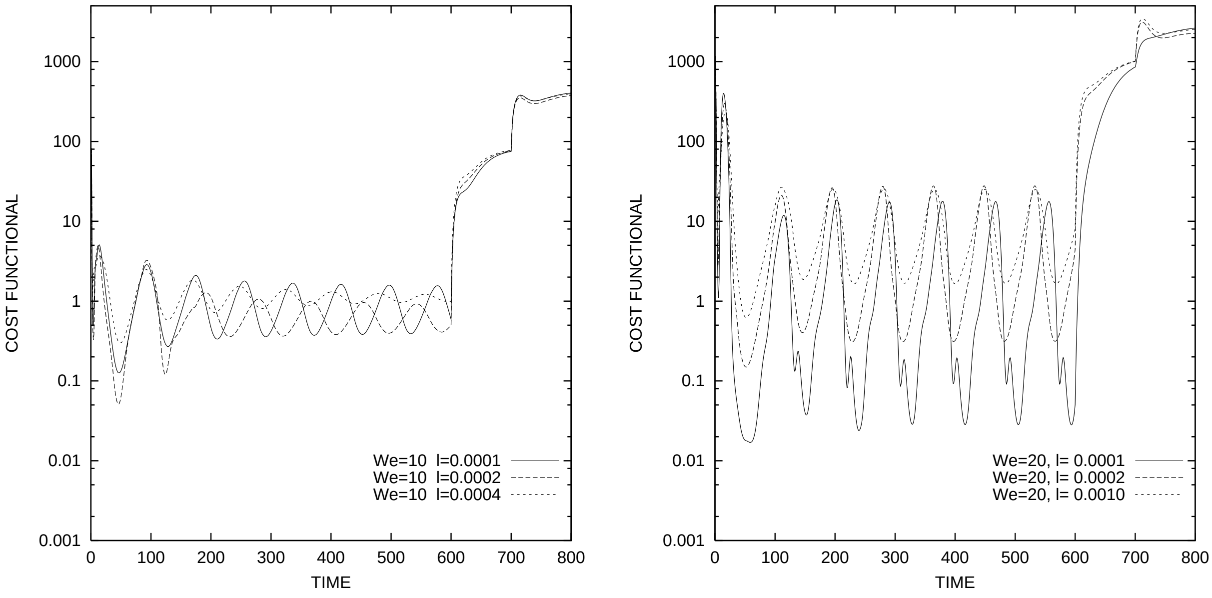

Fig 9: Cost functional for We = 10 (left) and We = 20 (right) with different choice of parameter ℓ.

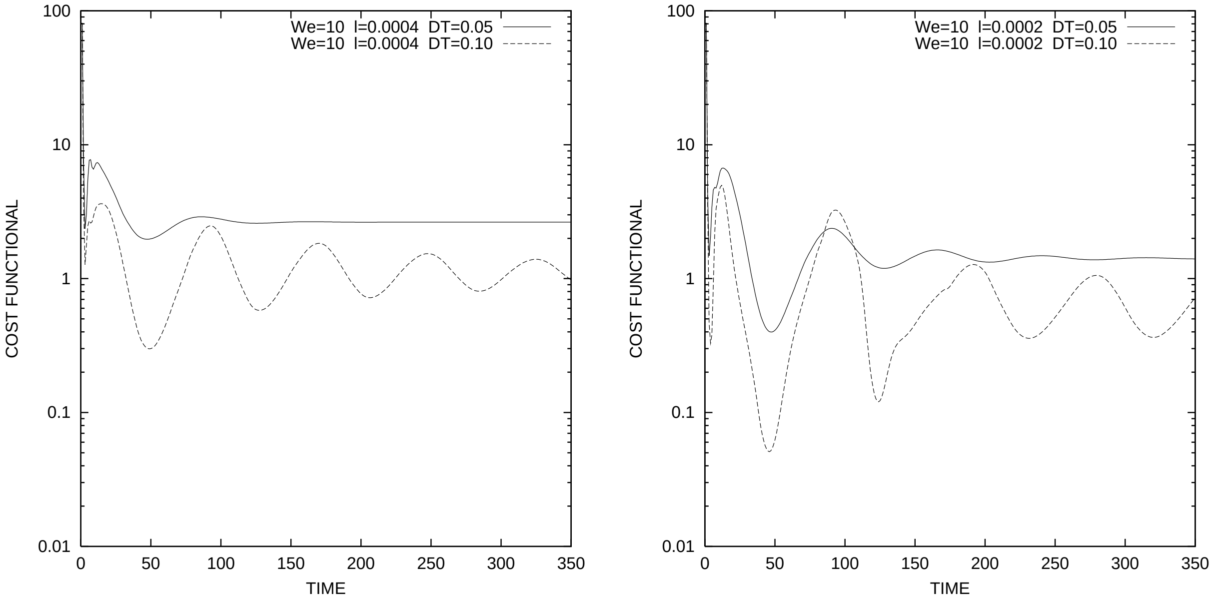

Fig 10: Cost functional until time $t = 400.0$ with $\Delta t = 0.10$ and $\Delta t = 0.05$ for We $= 10$, $\ell = 10^{-4}$ (left), We $= 10$, $\ell = 2 \times 10^{-4}$ (right)

no more active. In the simulation for Figures 5-7 the constraints were active only during the first time interval. Finally we give 2 snapshots of the simulation with We $=20$ and $\ell = 10^{-4}$, the first when the cost is at the maximum of the oscillations (Figure 11), the second when the cost is at the minimum of the oscillations (Figure 12). The intensity in the vortex (the maximal value of the stream function in the vortex) is reduced from $\phi = 1.0115$ to $\phi = 1.0012$ ($t = 380$) or $\phi = 1.0002$ ($t = 415$). Once again, this small decrease of the stream function intensity implies a strong decrease of the vortex size, as can be seen from the graphics: the reattachment length was X $= 0.178$ for the uncontrolled flow (Figure 4 right) and is X $= 0.125$ at time $t = 380$ and X $= 0.050$ at time $t = 415$.

6 Conclusions

In this work we investigated the ability of controlling transient viscoelastic fluid flows by heating or cooling a portion of the boundary of the flow domain. The sub-optimal instantaneous control strategy, with a gradient algorithm to minimise the cost functional, was found to be successful. Many factors account for the success of the procedure. Among them are the choice of the cost functional, the relative importance of the weights in the cost functional and the parameters of the gradient algorithm. After this initial feasibility study different and more sophisticated techniques could be employed. From the point of view of numerical optimization the gradient algorithm can be replaced by a conjugate gradient or possibly even a second order method. Modifications of the cost functional involving an appropriate measure for vorticity remain to be a worthwhile issue of investigation. Since the dynamics of the investigated flows appear to be "low dimensional", numerical realisation of the optimal control problem based on reduced order models could also be well suited. Finally, improvements could come from a better modeling of the flow with a more sophisticated thermal equation.

Acknowledgment : We are greatful to the referees for helpful comments and suggestions.

A Derivation of the optimality condition

We rewrite the equation on $\boldsymbol{\tau}$ by dividing all the terms by $\mathrm{We}(T)$:

$$[\frac{\partial \boldsymbol{\tau}}{\partial t} + (U \cdot \nabla)\boldsymbol{\tau} - \boldsymbol{\tau} \cdot \nabla U^T - \nabla U \cdot \boldsymbol{\tau}] + \frac{1}{\mathrm{We}(T)}[1 + \epsilon \frac{\mathrm{We}}{\omega_r} \mathrm{Tr}(\boldsymbol{\tau})]\boldsymbol{\tau} = 2\frac{\omega_r}{\mathrm{We}}\mathbf{D} \quad .$$

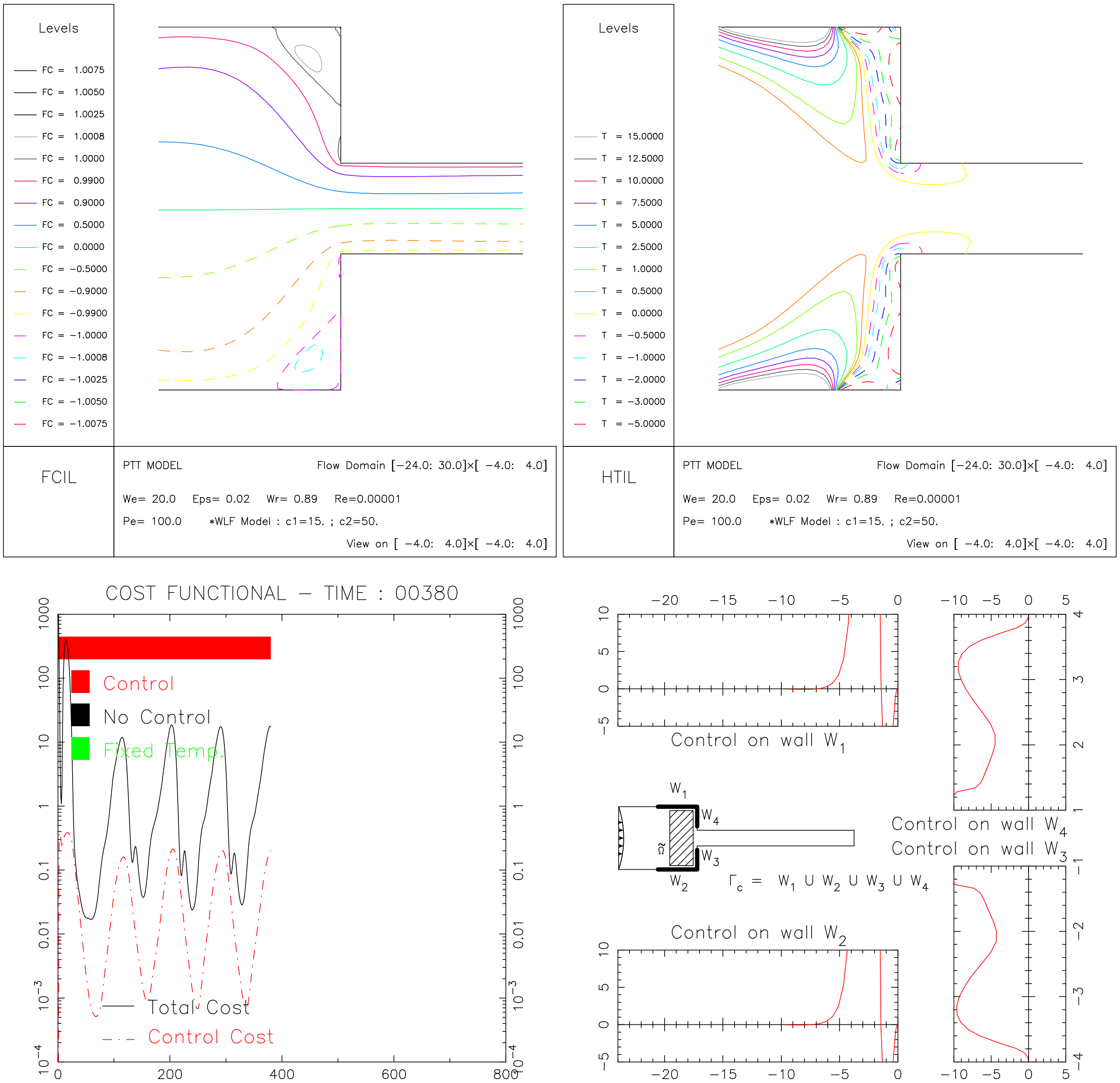

Fig 11: Simulation $\mathrm{We} = 20$, $\ell = 10^{-4}$ - Snapshot at $t = 380.0$

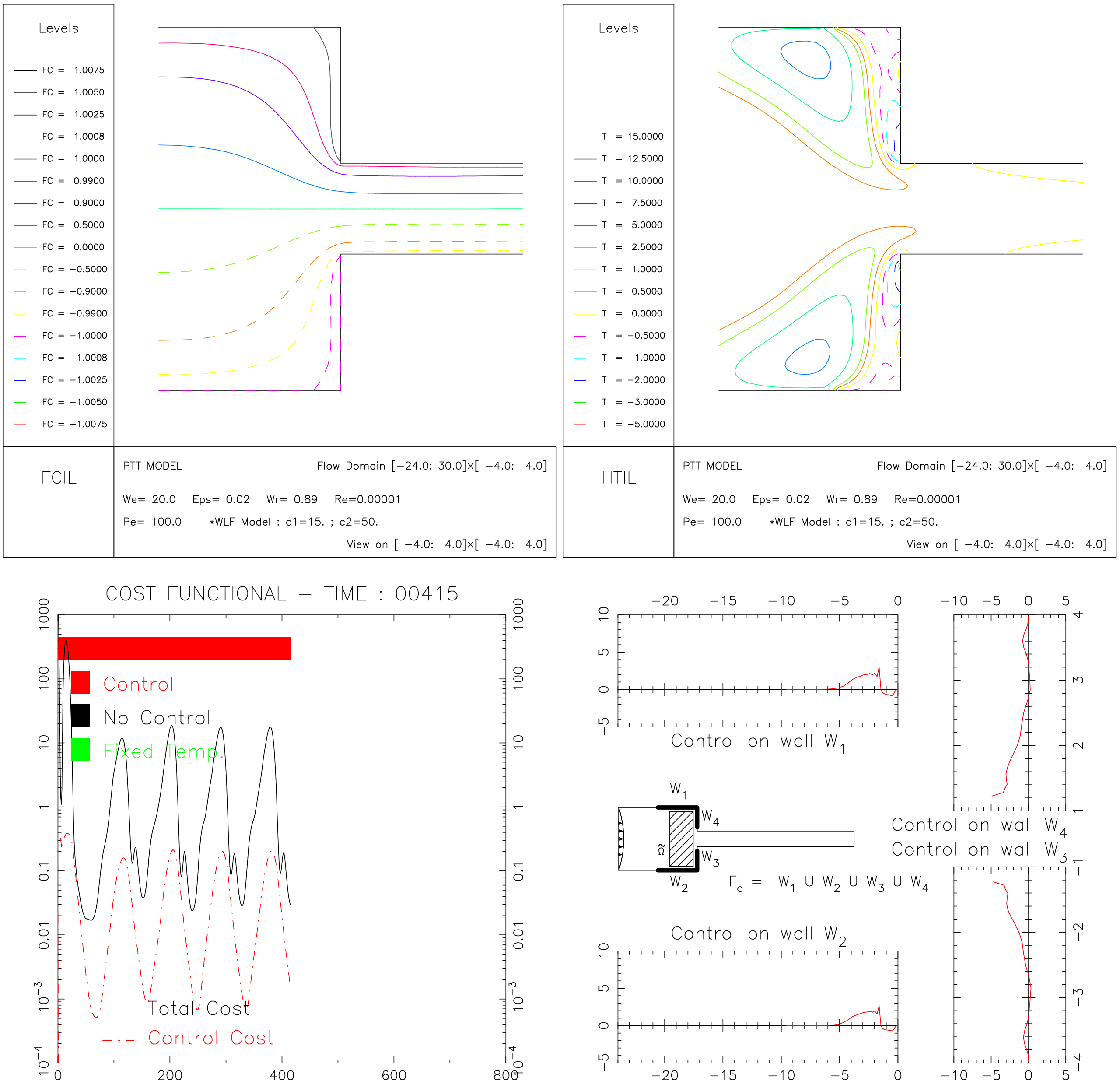

Fig 12: Simulation We $= 20$, $\ell = 10^{-4}$ - Snapshot at $t = 415.0$

The Lagrangian $\mathcal{L}$ for (opt) is given by :

$$\mathcal{L}(U,p,\boldsymbol{\tau},T,\mathbf{g},\mu,\xi,\pi,\boldsymbol{\theta},\rho,\lambda_i) \;=\; \mathcal{J}(U,\mathbf{g}) \;+$$

$$\int_0^{\mathfrak{T}}\int_\Omega \;[\mathrm{Re}(\frac{\partial U}{\partial t}+(U\cdot\nabla)U\;)-(1-\omega_r)\Delta U+\nabla p-\mathrm{Div}(\boldsymbol{\tau})\;]\cdot\xi\;dxdt\;+$$

$$\int_0^{\mathfrak{T}}\int_\Omega \;\mathrm{Div}(U)\;.\;\pi\;dxdt\;\;+$$

$$\int_0^{\mathfrak{T}}\int_\Omega \;[\frac{\partial \boldsymbol{\tau}}{\partial t}+(U\cdot\nabla)\boldsymbol{\tau}-\boldsymbol{\tau}\cdot\nabla U^T-\nabla U\cdot\boldsymbol{\tau}+\frac{1}{\mathrm{We}(T)}(1+\epsilon\frac{\mathrm{We}}{\omega_r}\mathrm{Tr}(\boldsymbol{\tau}))\boldsymbol{\tau}-2\frac{\omega_r}{\mathrm{We}}\mathbf{D}\;]:\;\boldsymbol{\theta}\;\;dxdt\;+$$

$$\int_0^{\mathfrak{T}}\int_\Omega \;[\frac{\partial T}{\partial t}+(U\cdot\nabla)T-\frac{1}{\mathrm{Pe}}\Delta T\;].\rho\;dxdt\;\;+$$

$$\int_0^{\mathfrak{T}}\int_{\Gamma_c}(T-\mathbf{g}).\mu\;d\Gamma_c dt\;+\;\int_0^{\mathfrak{T}}\int_{\Gamma_{in}}T.\lambda_1 d\Gamma_{in}dt\;+\;\int_0^{\mathfrak{T}}\int_{\Gamma_n}(\frac{\partial T}{\partial n}.\lambda_2)\;d\Gamma_n dt\;+$$

$$\int_0^{\mathfrak{T}}\int_{\Gamma_{in}}(\boldsymbol{\tau}-\boldsymbol{\tau}_P).\lambda_3\;d\Gamma_{in}dt\;+\;\int_0^{\mathfrak{T}}\int_{\Gamma}(U-U_b).\lambda_4\;d\Gamma dt\;\;.$$

For all $(\delta U,\delta p,\delta\boldsymbol{\tau},\delta T,\delta\mathbf{g})$, we must have :

$$\mathcal{L}_U(\delta U)+\mathcal{L}_p(\delta p)+\mathcal{L}_{\boldsymbol{\tau}}(\delta\boldsymbol{\tau})+\mathcal{L}_T(\delta T)+\mathcal{L}_{\mathbf{g}}(\delta\mathbf{g})=0 \quad , \tag{A.1}$$

where subscripts denote partial derivatives. We find

$$\mathcal{L}_p(\delta p) \;=\; +\int_0^{\mathfrak{T}}\int_\Omega \;\nabla(\delta p)\cdot\xi\;dxdt \tag{A.2}$$

$$\;=\; -\int_0^{\mathfrak{T}}\int_\Omega \;\delta p\;.\;\mathrm{div}\;\xi\;dxdt\;\;+\;\;\int_0^{\mathfrak{T}}\int_\Omega \;\delta p\;.\;(\xi\cdot\vec{n})\;d\Gamma dt\quad . \tag{A.3}$$

Choosing $\delta U=\delta\boldsymbol{\tau}=\delta T=0$ and δp with compact support in $\Omega\times[0:\mathfrak{T}]$, we obtain

$$\mathrm{div}\;\xi=0 \qquad \text{in } \Omega\times[0:\mathfrak{T}]\;\;.$$

Further we find

$$
\begin{aligned}
\mathcal{L}_U(\delta U) \;=\; & + \int_0^{\mathfrak{T}}\int_\Omega \; \mathcal{J}_U \cdot \delta U \; dxdt \\
& + \int_0^{\mathfrak{T}}\int_\Omega \; [\mathrm{Re}(\frac{\partial(\delta U)}{\partial t} + (U\cdot\nabla)\delta U \;+\; (\delta U\cdot\nabla)U) \;-(1-\omega_r)\Delta\delta U]\cdot\xi \; dxdt \\
& + \int_0^{\mathfrak{T}}\int_\Omega \; \mathrm{div}\;\delta U.\pi \; dxdt \\
& + \int_0^{\mathfrak{T}}\int_\Omega \; [\;(\delta U\cdot\nabla)\boldsymbol{\tau} - \boldsymbol{\tau}\cdot\nabla\delta U^T - \nabla\delta U\cdot\boldsymbol{\tau} \;-2\frac{\omega_r}{\mathrm{We}}\mathbf{D}(\delta U)] : \boldsymbol{\theta} \; dxdt \\
& + \int_0^{\mathfrak{T}}\int_\Omega \; (\delta U\cdot\nabla)T \;.\; \rho \; dxdt \quad + \int_0^{\mathfrak{T}}\int_\Omega \;\; \delta U\cdot\lambda_4 \; d\Gamma dt \qquad .
\end{aligned}
$$

Integration by part leads to :

$$
\begin{aligned}
\mathcal{L}_U(\delta U) \;=\; & + \int_0^{\mathfrak{T}}\int_\Omega \; \mathcal{J}_U \cdot \delta U \; dxdt \\
& - \int_0^{\mathfrak{T}}\int_\Omega \; \delta U\cdot\mathrm{Re}\;\frac{\partial\xi}{\partial t}\; dxdt + \int_\Omega [U(t=\mathfrak{T})\cdot\xi(t=\mathfrak{T}) \;-\; U(t=0)\cdot\xi(t=0)]\; dx \\
& - \int_0^{\mathfrak{T}}\int_\Omega \; \delta U\cdot\mathrm{Re}(U\cdot\nabla)\xi \; dxdt + \int_0^{\mathfrak{T}}\int_\Gamma \delta U\cdot\xi\mathrm{Re}(U\cdot\vec{n}) \; d\Gamma dt \\
& + \int_0^{\mathfrak{T}}\int_\Omega \delta U\cdot(\mathrm{Re}\nabla U^T\cdot\xi) \; dxdt \\
& - \int_0^{\mathfrak{T}}\int_\Omega (1-\omega_r)\delta U\cdot\Delta\xi \; dxdt - \int_0^{\mathfrak{T}}\int_\Gamma (1-\omega_r)\;[\;\partial_n\delta U\cdot\xi \quad - \quad \delta U\cdot\partial_n\xi\;]\; d\Gamma dt \\
& - \int_0^{\mathfrak{T}}\int_\Omega \delta U\cdot\nabla\pi \; dxdt \;+ \int_0^{\mathfrak{T}}\int_\Gamma (\delta U\cdot\vec{n})\;\pi\; d\Gamma dt \\
& + \int_0^{\mathfrak{T}}\int_\Omega \delta U\cdot[(\begin{array}{c}\partial_x\boldsymbol{\tau} : \boldsymbol{\theta}\\ \partial_y\boldsymbol{\tau} : \boldsymbol{\theta}\end{array})]\; dxdt \\
& + \int_0^{\mathfrak{T}}\int_\Omega \delta U\cdot[\;\mathrm{Div}\;(\boldsymbol{\theta}^T\;\boldsymbol{\tau})] + \mathrm{Div}\;(\boldsymbol{\theta}\;\boldsymbol{\tau}^T)\; dxdt \;- \int_0^{\mathfrak{T}}\int_\Gamma (n\delta U) : (\boldsymbol{\theta}^T\boldsymbol{\tau} + \boldsymbol{\tau}\;\boldsymbol{\theta}^T)\; d\Gamma dt \\
& + \int_0^{\mathfrak{T}}\int_\Omega 2\frac{\omega_r}{\mathrm{We}}(\delta U)\cdot\mathrm{Div}\;\boldsymbol{\theta}\; dxdt \;- \int_0^{\mathfrak{T}}\int_\Gamma 2\frac{\omega_r}{\mathrm{We}}\boldsymbol{\theta} : (\delta U\; n)\; d\Gamma dt \\
& + \int_0^{\mathfrak{T}}\int_\Omega \delta U\cdot(\rho.\nabla T)\; dxdt + \int_0^{\mathfrak{T}}\int_\Gamma \;\delta U\cdot\lambda_4\; d\Gamma dt \quad .
\end{aligned}
$$

Choosing δU with compact support in Ω, all boundary terms vanish and the last equality implies that

$$
-\,\mathrm{Re}\;\frac{\partial\xi}{\partial t} \;-\; \mathrm{Re}\;(U\cdot\nabla)\xi \;+\; \mathrm{Re}\;\nabla U^T\cdot\xi \;-\; (1-\omega_r)\Delta\xi \;-\; \nabla\pi \;+\; \mathcal{J}_U \;+\; (\begin{array}{c}\partial_x\boldsymbol{\tau} : \boldsymbol{\theta}\\ \partial_y\boldsymbol{\tau} : \boldsymbol{\theta}\end{array})
$$

$$- 2 \text{ Div } (\boldsymbol{\theta\tau}) \ - \ \rho \ \nabla T \ \ = 0 \quad .$$

We have also :

$$\xi(t = \mathfrak{T}) = 0 \quad .$$

Next boundary conditions on ξ are obtained restricting δU such that $\delta U = 0$ on Γ :

$$-(1-\omega_r) \int_0^{\mathfrak{T}} \int_\Gamma \partial_n \delta U \cdot \xi \ dxdt = 0 \quad .$$

So $\xi = 0$ on $\Gamma \times [0 : \mathfrak{T}]$ follows.

Taking variations with respect to $\delta\boldsymbol{\tau}$ we obtain :

$$\begin{aligned}
\mathcal{L}_{\boldsymbol{\tau}}(\delta\boldsymbol{\tau}) \ = \ & + \int_0^{\mathfrak{T}} \int_\Omega -\text{Div } \delta\boldsymbol{\tau} \cdot \xi \ dxdt \\
& + \int_0^{\mathfrak{T}} \int_\Omega [\frac{\partial(\delta\boldsymbol{\tau})}{\partial t} + (U \cdot \nabla)\delta\boldsymbol{\tau} - \delta\boldsymbol{\tau} \cdot \nabla U^T - \nabla U \cdot \delta\boldsymbol{\tau}] : \boldsymbol{\theta} \ dxdt \\
& + \int_0^{\mathfrak{T}} \int_\Omega [\frac{\delta\boldsymbol{\tau}}{We(T)} + \epsilon \frac{\text{We}}{\omega_r} \frac{1}{We(T)} (\text{Tr}(\delta\boldsymbol{\tau})\boldsymbol{\tau} + \text{Tr}(\boldsymbol{\tau})\delta\boldsymbol{\tau})] : \boldsymbol{\theta} \ dxdt \quad .
\end{aligned}$$

With the rules of calculus and integration by parts we calculate :

$$\begin{aligned}
\mathcal{L}_{\boldsymbol{\tau}}(\delta\boldsymbol{\tau}) \ = \ & + \int_0^{\mathfrak{T}} \int_\Omega \delta\boldsymbol{\tau} : \nabla\xi \ dxdt \ - \ \int_0^{\mathfrak{T}} \int_\Omega \delta\boldsymbol{\tau} : (\xi\vec{n}) \ dxdt \\
& - \int_0^{\mathfrak{T}} \int_\Omega \delta\boldsymbol{\tau} : \frac{\partial\boldsymbol{\theta}}{\partial t} \ dxdt \ + \ \int_\Omega [(\boldsymbol{\tau} : \boldsymbol{\theta})(t = \mathfrak{T}) - (\boldsymbol{\tau} : \boldsymbol{\theta})(t = 0)] \ dx \\
& - \int_0^{\mathfrak{T}} \int_\Omega \delta\boldsymbol{\tau} : (U \cdot \nabla)\boldsymbol{\theta} \ dxdt \ + \ \int_0^{\mathfrak{T}} \int_\Gamma \delta\boldsymbol{\tau} : (U \cdot \vec{n})\boldsymbol{\theta} \ d\Gamma dt \\
& + \int_0^{\mathfrak{T}} \int_\Omega \delta\boldsymbol{\tau} : (\boldsymbol{\theta} \cdot \nabla U + \nabla U^T \cdot \boldsymbol{\theta}) \ dxdt \\
& + \int_0^{\mathfrak{T}} \int_\Omega \delta\boldsymbol{\tau} : \frac{\boldsymbol{\theta}}{We(T)} \ dxdt \ + \ \epsilon \frac{\text{We}}{\omega_r} \int_0^{\mathfrak{T}} \int_\Omega \delta\boldsymbol{\tau} : \frac{1}{We(T)} [\text{Tr}(\boldsymbol{\tau})\boldsymbol{\theta} + (\boldsymbol{\tau} : \boldsymbol{\theta})\mathbf{I}] \ dxdt \\
& + \int_0^{\mathfrak{T}} \int_{\Gamma_{in}} \delta\boldsymbol{\tau} : \lambda_3 \ d\Gamma_{in} dt \quad .
\end{aligned}$$

The equation for $\boldsymbol{\theta}$ is :

$$\text{We}(T)[-\frac{\partial\boldsymbol{\theta}}{\partial t} - (U \cdot \nabla)\boldsymbol{\theta} - \ \boldsymbol{\theta} \cdot \nabla U \ + \ \nabla U^T \cdot \boldsymbol{\theta} \ ] + \boldsymbol{\theta} + \epsilon \frac{\text{We}}{\omega_r} [\text{Tr}(\boldsymbol{\tau})\boldsymbol{\theta} + (\boldsymbol{\tau} : \boldsymbol{\theta})\mathbf{I}] = - \ \text{We}(T).\mathbf{D}(\xi) \ ,$$

and we have :

$$\boldsymbol{\theta}(t = \mathfrak{T}) = 0 \quad .$$

Boundary conditions on $\boldsymbol{\theta}$:

If $\xi \ = \ 0$ on Γ, then for all $\delta\boldsymbol{\tau}$ we have :

$$\delta\boldsymbol{\tau} \ : \ [\lambda_3 . \chi_{\Gamma_{in}} \ + \ (U \cdot \vec{n}) \ \boldsymbol{\theta} \ ] = 0 \quad \text{ for all } x \text{ and } t.$$

This implies that $\boldsymbol{\theta} = 0$ on $\Gamma_{out} \times [0 : \mathfrak{T}]$ since $U \cdot \vec{n} \neq 0$ there. Since $U \cdot \vec{n} = 0$ on $\Gamma \backslash (\Gamma_{in} \cup \Gamma_{out})$, there is no boundary conditions for $\boldsymbol{\theta}$ on $(\Gamma \backslash (\Gamma_{in} \cup \Gamma_{out})) \times [0 : \mathfrak{T}]$. On Γ_{in} as well $\boldsymbol{\theta}$ does not satisfy boundary conditions and $\lambda_3 = -(U \cdot \vec{n})\boldsymbol{\theta}$ there.

Taking variations with respect to δT we find

$$\begin{aligned}
\mathcal{L}_T(\delta T) \ = \ & + \int_0^{\mathfrak{T}}\int_\Omega [\frac{\partial(\delta T)}{\partial t} + (U \cdot \nabla)\delta T - \frac{1}{\text{Pe}}\Delta \delta T] \ . \ \rho \ dxdt \\
& + \int_0^{\mathfrak{T}}\int_\Omega (\frac{1}{\text{We}})'(T)[\delta T(\boldsymbol{\tau} + \epsilon\frac{\text{We}}{\omega_r}\text{Tr}(\boldsymbol{\tau})\boldsymbol{\tau}) \ ] : \boldsymbol{\theta} \ dxdt \\
& + \int_0^{\mathfrak{T}}\int_{\Gamma_c} \delta T \ . \ \mu \ d\Gamma_c dt \ + \ \int_0^{\mathfrak{T}}\int_{\Gamma_{in}} \delta T . \lambda_1 \ d\Gamma_{in} dt \ + \ \int_0^{\mathfrak{T}}\int_{\Gamma_n} \partial_n(\delta T) . \lambda_2 \ d\Gamma_n dt \ = \ 0 \quad ,
\end{aligned}$$

and further

$$\begin{aligned}
\mathcal{L}_T(\delta T) \ = \ & - \int_0^{\mathfrak{T}}\int_\Omega \delta T \ . \ \frac{\partial \rho}{\partial t} \ dxdt \ + \ \int_\Omega [\ (\rho T)(t = \mathfrak{T}) \ dx \ - \ (\rho T)(t = 0) \ ] \ dxdt \\
& - \int_0^{\mathfrak{T}}\int_\Omega \delta T \ . \ (U \cdot \nabla)\rho \ dxdt \ + \int_0^{\mathfrak{T}}\int_\Gamma \delta T \ . \ (U \cdot \vec{n}) \ \rho \ d\Gamma dt \\
& - \int_0^{\mathfrak{T}}\int_\Omega \delta T \ . \ \frac{1}{\text{Pe}}\Delta\rho \ dxdt \ - \int_0^{\mathfrak{T}}\int_\Gamma \frac{1}{\text{Pe}}[\ \partial_n(\delta T) \ . \ \rho \ \ - \ \delta T \ . \ \partial_n \rho \ ] \ d\Gamma \\
& + \int_0^{\mathfrak{T}}\int_\Omega \delta T \ (\frac{1}{\text{We}})'(T)[1 + \epsilon\frac{\text{We}}{\omega_r}\text{Tr}(\boldsymbol{\tau})]\boldsymbol{\tau} : \boldsymbol{\theta} \ dxdt \\
& + \int_0^{\mathfrak{T}}\int_{\Gamma_c} \delta T . \ \mu \ d\Gamma_c \ dt \ + \int_0^{\mathfrak{T}}\int_{\Gamma_{in}} \delta T . \ \lambda_1 \ d\Gamma_{in} dt \ + \int_0^{\mathfrak{T}}\int_{\Gamma_n} \partial_n(\delta T) . \lambda_2 \ d\Gamma_n dt \ = \ 0 \quad ,
\end{aligned}$$

which implies, for δT with support compact in Ω :

$$-\frac{\partial \rho}{\partial t} \ - \ (U \cdot \nabla)\rho \ - \ \frac{1}{\text{Pe}}\Delta\rho \ + \ (\frac{1}{\text{We}})'(T)[1 + \epsilon\frac{\text{We}}{\omega_r}\text{Tr}(\boldsymbol{\tau})]\boldsymbol{\tau} : \boldsymbol{\theta} \ = 0 \quad .$$

We must also have :

$$\rho(t = \mathfrak{T}) = 0 \quad .$$

Boundary conditions on ρ :

When choosing δT such that $\partial_n \delta T \ = 0$, we obtain

$$(\ \delta T \ , \ (U \cdot \vec{n})\rho \ )_\Gamma \ + \ \frac{1}{\text{Pe}}(\ \delta T \ , \ \partial_n \rho)_\Gamma \ + \ (\ \delta T \ , \ \mu \ )_{\Gamma_c} \ + \ (\ \delta T \ , \ \lambda_1 \ )_{\Gamma_{in}} = 0 \quad , \qquad \text{(A.4)}$$

and then

$$(U \cdot \vec{n})\rho \;+\; \frac{1}{\mathrm{Pe}}\,\partial_n \rho \;+\; \mu.\chi_c \;+\; \lambda_1.\chi_{in} \;=0 \quad . \tag{A.5}$$

Considering $\Gamma \backslash (\Gamma_c \cup \Gamma_{in})$, we have :
If $U \cdot \vec{n} = 0$ then $\partial_n \rho = 0$ (ie on fixed walls minus Γ_c).
If $U \cdot \vec{n} \neq 0$ then $\frac{1}{\mathrm{Pe}}\partial_n \rho + u\rho = 0$ (ie on Γ_{out}).

When choosing δT such that $\delta T \;=0$ on Γ, we obtain

$$-\frac{1}{\mathrm{Pe}}(\;\partial_n \delta T \;,\; \rho\;)_\Gamma \;+\; (\;\partial_n \delta T \;,\; \lambda_2\;)_{\Gamma_n} \;=\; 0 \tag{A.6}$$

So that outside Γ_n we have $\rho = 0$.

In addition, we have on Γ_c : $\mu \;+\; \frac{1}{\mathrm{Pe}}\partial_n \rho \;=0$, which gives the optimality condition :

$$(OC) \qquad \ell.\mathbf{g} = -\frac{1}{\mathrm{Pe}}\partial_n \rho \quad \text{on } \Gamma_c \;\text{ for all } t \in [0:\mathfrak{T}] \quad . \tag{A.7}$$

Finally we have

$$\mathcal{L}_{\mathbf{g}}(\delta \mathbf{g}) = \int_0^{\mathfrak{T}}\!\!\int_{\Gamma_c} \ell\;\mathbf{g}.\delta g\; d\Gamma_c dt \;-\int_0^{\mathfrak{T}}\!\!\int_{\Gamma_c} \delta\mathbf{g}.\mu\; d\Gamma_c dt = 0 \quad , \tag{A.8}$$

which is equivalent to

$$\mu = \ell.\mathbf{g} \qquad \text{on } \;\Gamma_c \times [0:\mathfrak{T}] \quad . \tag{A.9}$$

References

[1] F.T.P. Baaijens et al. "Viscoelastic flow past a confined cylinder of low density polyethylene melt". Journal of Non-Newtonian Fluid Flows, 68(1997),173-204.

[2] F.T.P. Baaijens. "An iterative solver for the DEVSS/DG method with application to smooth and non-smooth flows of the upper convected Maxwell fluid" Journal of Non-Newtonian Fluid Flows, 75(1998),119-138.

[3] C. Beraudo et al. "A finite element method for computing the flow of multi-mode viscoelastic fluids: comparison with experiments" Journal of Non-Newtonian Fluid Flows, 75(1998),1-23.

[4] T. Bewley, P. Moin and R. Temam. "DNS-based predictive control of turbulence: an optimal benchmark for feedback algorithms" Under consideration for publication in J. Fluid Mech.

[5] H. Choi, M. Hinze, K. Kunisch. "Instantaneous control of backward-facing step flows". Preprint No 571, Technical University Berlin, Germany.

[6] H. Choi, R. Temam, P. Moin and J. Kim. "Feedback control for unsteady flow and its application to the stochastic Burgers equation". J. Fluid Mech. 253(1993),509-543.

[7] S. Dupont and M.J. Crochet. "The vortex growth of a KBKZ fluid in an abrupt contraction". Journal of Non-Newtonian Fluids Mechanics, 29(1988),81-91.

[8] Y. Fan, R.I. Tanner, N. Phan-Tien. "Galerkin/least square finite-element methods for steady viscoelastic flows" Journal of Non-Newtonian Fluids Mechanics, 84(1999),233-256.

[9] M.A. McClelland and B.A. Finlayson. "Heat Transfer effects in extrudate swell of elastic liquids". Journal of Non-Newtonian Fluid Mechanics, 27(1988),363-374.

[10] R. Guenette and M. Fortin. "A new mixed finite element method for computing viscoelastic flows". Journal of Non-Newtonian Fluid Flows, 62(1995),27-52.

[11] J.W. He, R. Glowinski, M. Gorman and J. Periaux. "Some results on the controllability and the stabilisation of the Kuramoto-Sivashinsky equation", preprint.

[12] K. Ito and S.S. Ravindran. "A reduced order method for simulation and control of fluid flows". J. Computational Physics, 1997 (Submitted).

[13] K. Ito and S.S. Ravindran. "A reduced basis method for control problems governed by PDE's". Proceedings of control theory for distributed parameters systems, Birkhauser Verlag, Basel,pp. 173-191, 1997.

[14] K. Ito and S.S. Ravindran. "Reduced basis method for optimal control of unsteady viscous flows". Preprint, Department of Mathematics, North Carolina State University, USA, 1997.

[15] K. Kunisch and X. Marduel. "Optimal control of non-isotherm viscoelastic fluid flows". Journal of Non-Newtonian Fluid Mechanics, accepted.

[16] M. Hinze, K. Kunisch. "Suboptimal control strategies for backwards facing step flows". Proceedings of 15th IMACS World Congress on Scientific Computation, Modelling and Applied Mathematics, Editor A. Sydow, Vol. 3, 53-58, 1997.

[17] K. Kunisch and S. Volkwein. "Control of Burger's equation by a reduced order Approach using proper orthogonal decomposition". Preprint SFB No 138, K.F. Universität Graz, Autria.(accepted for publication in JOTA)

[18] K. Kunisch and M. Hinze. "Second Order Method for Optimal Control of Time Dependent Fluid Flow". Preprint SFB, K.F. Universität Graz, Autria.

[19] X.L. Luo and R.I Tanner. "A pseudo-time integral method for non-isothermal viscoelastic flows and its application to extrusion simulation". Rheology Acta 26(1987),499-507.

[20] X. Marduel. These de doctorat de l'Université Paris-Sud Orsay. "Simulations Numeriques d'écoulements de fluides viscoelastiques".

[21] G.W.M. Peters and F.T.P. Baaijens. "Modelling of non-isothermal viscoelastic flows" Journal of Non-Newtonian Fluid Mechanics, 68 (1997),205-224.

[22] J.S. Peterson. "The reduced basis method for incompressible viscous flow calculations". SIAM J. Sci. Stat. Comput., 10(1989)777-786.

[23] P. Saramito. "Efficient simulation of non-linear viscoelastic flows". Journal of Non-Newtonian Fluids Mechanics, 60(1995),199-223.

[24] F. Sugend, N. Phan-Thien and R.I. Tanner. "A study of Non-Isothermal Non-Newtonian Extrudate Swell by a Mixed Boundary Element and Finite Element Method". Journal of Rheology 31(1)(1987),37-58.

[25] K.Y. Tang, W.R. Graham, J. Peraire. "Active flow control using a reduced order method and optimum control". AIAA-1946, 1996.

[26] R.I. Tanner. "Engineering Rheology". Oxford University Press, London, 1985

[27] C.L. Tucker. "Fundamentals of computer modelling for polymer processing". Hanser Publishers (1989).

[28] J.M. Wiest and N. Phan-Thien. "Non-Isothermal Flow of Polymer Melts". Journal of Non-Newtonian Fluid Mechanics, 27(1989),333-347.

[29] M.L. Williams, R.F. Landel, and J.D. Ferry. J. Am. Chem. Soc.,77(1955),3701.

[30] R. Zheng et al. "Thermoviscoelastic simulation of thermally and pressure-induced stresses in injection moulding for the prediction of shrinkage and warpage for the fibre-reinforced thermoplatics" Journal of Non-Newtonian Fluid Mechanics, 84(1999),159-190.